

Methods for Measuring the Acoustic Response of Wind Instruments

Alexander Buckiewicz-Smith



Music Technology Area, Department of Theory
Schulich School of Music
McGill University
Montreal, Quebec, Canada

February 2008

A thesis submitted to McGill University in partial fulfillment of the requirements for the degree of Master of Arts in Music Technology.

© 2008 Alexander Buckiewicz-Smith

Abstract

This thesis studies methods to take acoustical measurements of wind instrument bodies and mouthpieces. Acoustic responses and existing measurement methods are reviewed. Multiple- and single-microphone measurement techniques are compared with a discussion of object-length limitations and frequency response.

Impulse response measurements using a complex input signal are discussed and signals used for measuring room acoustics are reviewed. Construction and deconvolution methods for several types of signals are specified and the effects of signal degradation on measurements are discussed.

A novel pulse reflectometry technique that can use these signals as stimulus is presented. The signals are used in a waveguide model which simulates adverse measurement scenarios and calculated impedances are compared. Model measurements are then compared with actual reflection function measurements of two fabricated test objects to show the limitations of pulse reflectometry when calculating the impedance of long objects.

Viscothermal losses and open-end radiation characteristics measured using a pulse reflectometry setup are then compared with their theoretically predicted values. Finally, the input impedance calculated from several saxophone mouthpieces are presented and a novel method for measuring the reed resonance frequency of a mouthpiece is shown.

Résumé

Cette thèse étudie des méthodes pour prendre des mesures acoustiques des corps et embouchures d'instruments à vent. Les réponses acoustiques et les méthodes existantes de mesure sont passées en revue. Mesures de multiples pressions et pression unique sont contrastées par une discussion des limitations sur la longueur de l'objet et la réponse en fréquences.

Les mesures de réponse d'impulsion employant un signal d'entrée complexe sont discutées et des signaux utilisés pour mesurer l'acoustique de salles sont passés en revue. Les méthodes de construction et de déconvolution pour plusieurs types de signaux sont spécifiés et les façons dont la dégradation des signaux affecte les mesures sont discutées.

Une nouvelle technique de réflectométrie d'impulsion qui peut employer ces signaux comme stimulus est présentée. Les signaux sont employés dans un modèle de guide d'ondes qui simule les scénarios défavorables de mesures et calculent les impédances. Des mesures de modèles sont alors comparées aux mesures réelles de fonction de réflexion de deux prototypes fabriqués pour montrer les limitations de la réflectométrie d'impulsion lors de calculs de l'impédance de longs objets.

Les pertes viscothermiques et les caractéristiques de rayonnement d'extrémité ouverte mesurées en utilisant une installation de réflectométrie d'impulsion sont alors comparées à leurs valeurs théoriques prévues. En conclusion, l'impédance d'entrée calculée à partir de plusieurs embouchures de saxophones sont présentées ainsi qu'une nouvelle méthode pour mesurer la fréquence tubulaire de résonance d'une embouchure.

Acknowledgments

Thanks first to my supervisor Dr. Gary Scavone for his advice, encouragement and wise direction. His help selecting a field of study and advice how to best explore the topic made the work relevant; his experience coupled with his kind manner made it possible.

For all of his assistance performing the measurements I would like to thank Antoine Lefebvre. In addition to machining all the parts for the pulse reflectometry setup he compared pulse reflectometry measurements with ones using a multiple-microphone technique, enhancing the quality of the research results.

Much of my understanding of this field is a result of the sage advice and enriching conversations that I had with Dr. Jonathan Abel about impulse response and impedance measurements. I am grateful for his careful explanations and technical assistance working out many of the techniques described in the paper.

For answering the multitude of small queries and questions that occurred to me throughout this research, I am extremely thankful for the insightful advice and suggestions of all of the members of the Music Technology Area, and particularly the members of the CAML lab. The technical direction and help given by Mark Zadel, Andrey da Silva, Dave Benson and Darryl Cameron in particular were instrumental in allowing me to finish this work. Special thanks to Denis Lebel for assistance with writing and his enthusiastic and engaging conversation.

I am also deeply indebted to my incredible family. Their support throughout my studies and the successes they've achieved were a constant inspiration. None of this work would have been possible without their encouragement and devotion.

Contents

1	Introduction	1
1.1	Motivation	1
1.2	Outline	2
2	Wind Instrument Impedance Measurement Techniques	4
2.1	Volume Velocity Measurements	6
2.2	Multi-Microphone Methods	7
2.2.1	The Two-Microphone, Three-Calibration (TMTC) Technique	7
2.2.2	Two Microphone Technique Variations	8
2.2.3	Errors	9
2.3	Single-Microphone Methods	9
2.3.1	Measurement Setup	10
2.3.2	System Calibration	12
2.3.3	Measurement Procedure	13
2.3.4	Measuring Long Reflectances	13
2.3.5	Stimulus Length	14
2.4	Apparatus Issues	14
3	Stimulus Signals for Acoustic Measurements	16
3.1	Impulses and Periodic Pulses	17
3.2	Maximum Length Sequences (MLSs)	18
3.3	Golay Codes	20
3.4	Frequency-Domain Designed Noise	22
3.5	Swept Sines	23
3.6	All-Pass Sequences	25
3.7	Time Stretched Pulses	26
3.8	Refinements and Comparisons	28
3.8.1	Averaging	28
3.8.2	Pre-emphasis	28
3.8.3	Transient Noise	29
3.8.4	Non-linearity	29

3.8.5	Overall Comparisons	30
4	Pulse Reflectometry Improvements	31
4.1	Longer Stimulus Signals	31
4.1.1	Theory	31
4.1.2	Verification	32
4.1.3	Comparison of Stimulus Signals	35
4.2	Pulse Reflectometry Window Size Effects	43
4.2.1	Short Cylinder	44
4.2.2	Longer Cylinder	50
4.3	Conclusions	56
5	Impedance Measurement Results	57
5.1	Measurements	57
5.1.1	Viscothermal Losses	57
5.1.2	Open End Measurements	57
5.1.3	Mouthpiece Measurements	59
5.1.4	Mouthpiece Measurement Issues	61
6	Conclusions	63
6.1	Future Work	64

List of Figures

2.1	A basic two-port network.	5
2.2	A two-microphone measurement apparatus.	8
2.3	A pulse reflectometry apparatus.	11
2.4	The calibration measurement for a pulse reflectometry system showing $f(t)$, $f(t) * r_o(t)$ and $f(t) * r_o(t) * r_s(t)$	12
3.1	Time-domain signal and frequency-domain phase information for a Maximum Length Sequence (MLS).	19
3.2	Time-domain signal and frequency-domain phase information for a designed random noise signal.	22
3.3	Time-domain signal and frequency-domain phase information for a linearly swept sine.	23
3.4	Time-domain signal and frequency-domain phase information for a logarithmically swept sine.	24
3.5	The time-domain signal and frequency-domain magnitude and phase information for an All-Pass Sequence.	26
3.6	Time-domain signal and frequency-domain phase information for an Optimized Aoshima Time Stretched Pulse (OATSP).	27
4.1	The pressure signal from a pulse reflectometry calibration measurement when using repeated pulse testing.	33
4.2	The pressure signal from a pulse reflectometry calibration measurement when using a swept sine stimulus.	33
4.3	The impulse response of a calibration measurement of a pulse reflectometry system stimulated using repeated pulse testing (top) and swept sine testing (bottom) on a log scale.	34
4.4	The impulse response of a calibration measurement of a pulse reflectometry system stimulated using repeated pulse and swept sine testing on a linear scale.	35
4.5	The reflectance of the open-end filter approximating the results of Levine and Schwinger (1948).	36

4.6	The impedance of the open end filter calculated using the reflection function of Fig. 4.5.	37
4.7	Calculated impedance of the open end of a circular cylindrical pipe using noise in the presence of non-linear contamination.	38
4.8	Calculated impedance of the open end of a circular cylindrical pipe using a linearly swept sine in the presence of non-linear contamination.	39
4.9	Calculated impedance of the open end of a circular cylindrical pipe using an OATSP in the presence of non-linear contamination.	39
4.10	Calculated impedance of the open end of a circular cylindrical pipe using a repeated pulse testing in the presence of uncorrelated white noise.	40
4.11	Calculated impedance of the open end of a circular cylindrical pipe using an MLS in the presence of uncorrelated white noise.	41
4.12	Calculated impedance of the open end of a circular cylindrical pipe using a repeated pulse testing in the presence of a DC offset.	42
4.13	Calculated impedance of the open end of a circular cylindrical pipe using an OATSP in the presence of a DC offset.	42
4.14	The input impedance of a short cylinder predicted using a frequency-domain method plotted against the input impedance calculated from a waveguide model.	44
4.15	The input impedance of a short cylinder calculated from a waveguide model of a pulse reflectometry system that models a diameter discontinuity between the source tube and the cylinder.	45
4.16	The input impedance of a short cylinder calculated from a waveguide model of a pulse reflectometry system that models a diameter discontinuity between the source tube and the cylinder and a reflecting source.	46
4.17	The difference between the input impedance calculated from a pulse reflectometry model incorporating a diameter discontinuity and reflecting source and an ideal pulse reflectometry system	47
4.18	The input impedance of the short cylinder predicted from a frequency-domain model and calculated from measurements taken from a pulse reflectometry apparatus.	48
4.19	The magnitude difference between short cylinder input impedances calculated using a frequency domain model and those calculated from a pulse reflectometry apparatus	49
4.20	The input impedance of the short cylinder predicted from a frequency-domain model and calculated from measurements that incorporate source reflections taken from a pulse reflectometry apparatus.	50
4.21	The magnitude difference between short cylinder input impedances calculated using a frequency domain model and those calculated from a pulse reflectometry apparatus, including source reflections.	50

4.22	The input impedance of a long cylinder predicted using a frequency-domain model plotted against input impedance calculated from an ideal waveguide model.	51
4.23	The input impedance of the longer cylinder calculated from an ideal waveguide simulation and input impedance calculated from a waveguide modelling a reflecting source and a diameter discontinuity.	52
4.24	The magnitude difference between the input impedance calculated from an ideal waveguide simulation and input impedance calculated from a waveguide incorporating a reflecting source and scattering junction.	52
4.25	The input impedance of the longer cylinder calculated from an ideal waveguide simulation and the input impedance calculated by incorporating source reflections from a waveguide modelling a reflecting source and a diameter discontinuity.	53
4.26	The magnitude difference between the input impedance calculated from an ideal waveguide simulation and input impedance calculated by incorporating source reflections from a waveguide modelling a reflecting source and diameter discontinuity.	53
4.27	The input impedance of the long cylinder predicted from a frequency-domain model and calculated from measurements taken from a pulse reflectometry apparatus.	54
4.28	The magnitude difference between the input impedance predicted from a frequency-domain model of the long cylinder and the input impedance calculated from measurements taken from a pulse reflectometry apparatus.	54
4.29	The input impedance of the long cylinder predicted from a frequency-domain model and calculated from measurements taken from a pulse reflectometry apparatus.	55
4.30	The magnitude difference between long cylinder input impedances calculate using frequency domain model and measured from pulse reflectometry with a double-sized window.	56
5.1	Measured magnitude and phase losses over T_{M-O}	58
5.2	The reflectance magnitude and end length correction measured from the open end of the source tube.	58
5.3	Input impedances measured from Caravan, Meyer, Rascher and Selmer mouthpieces while the reed was held closed.	60
5.4	Input impedances from the Selmer mouthpiece while in various states.	61
5.5	Zoom in on the tail of the pressure response of the Selmer mouthpiece in various states.	61

Chapter 1

Introduction

1.1 Motivation

This thesis focuses on measuring the acoustics of wind instruments, such as saxophones, trumpets or clarinets. Input impedance is the most important and useful variable for characterizing acoustic spaces, including ducts, pipes and musical instruments, in a way that is independent of environment or playing conditions and acoustic studies of wind instruments concentrate on input impedance because this one measure informs many qualities of an instrument. Variation in instrument type, tone-color and manufacturer are expressed as differences in the input impedance and so by measuring impedance, it may be possible to gain greater insight into musical qualities of the instrument.

In scientific studies, acoustic measures of the instruments are taken in controlled settings so experiments can be repeated and finding can be verified. Because players can create such drastically different sounds, which can be difficult to reproduce, scientific studies use electrically driven speakers or other mechanical means that can consistently excite the instruments in the same manner. This measurement scenario does not encompass the full complexity of the interaction that occurs when the instrument is played, but gives a useful, broad impression of the instrument.

Our theoretical understanding of the physics and underlying musical acoustics can be refined and expanded by comparing accurate measures of the input impedance of real instruments to our predictions. Some theories of wind instrument physics remain unsupported by quantitative physical measurement and more accurate or flexible measurement techniques are needed to verify them. Besides pure research, systems that accurately measure impedance can also be used to test that fabricated instruments match their specifications, to test that the pads and dampers are correctly set up and to locate faults that require repairs, including dents, cracks and leaks.

Higher quality impedances from these measurements can also be used to set parameters for physical models, improving their accuracy. With more accurate measurements of similar objects, it should be possible to match quantitative differences in physical measures like

the input impedance to qualitative differences in musical aesthetics.

1.2 Outline

The thesis presented here explores some challenges when measuring input impedance and compares the strengths and weaknesses of existing measurement techniques as well as some possible improvements. Impulse response measurement techniques are also compared, with a focus on the qualities likely to affect their applicability to input impedance measurements. A theoretical basis for using impulse response measurement techniques to calculate input impedances is given and then verified experimentally. The effects of non-ideal measurement conditions on input impedances calculated using these different techniques are then modelled and compared to the theoretical predictions. Additionally, limits to the acoustical systems that can be measured are explored.

Chapter 2 will discuss the way wind instruments are modelled and some of the acoustical measurements of wind instruments that have been taken. The chapter describes setups used to take these measurements and general concerns when making measurements. A review is given of the ways to measure impedances by measuring volume velocity, including direct measurements and the use of multiple pressure sensors related to it, with discussion concerning the errors involved in those measures. Single microphone methods to measure time-domain reflection functions are then discussed with attention given to the current limits on the length of the stimulus signal and the object under test.

Chapter 3 is a review of stimulus signal types for acoustic measurements. The literature reviewed focuses on the use of these signals in room impulse response measurements and their benefits and drawbacks in these scenarios. The introduction discusses the use of complex input functions to measure the impulse response of a linear time-invariant system and a short discussion of how the periodic impulse response relates to the impulse response is given.

The stimulus signal types discussed include Maximum Length Sequences (MLSs), Golay codes, frequency-domain designed noise, swept sine waves, all-pass sequences and frequency-domain designed stretched pulse. An introduction to each signal type discusses how each signal is created, their time- and frequency-domain makeup and how deconvolution of each signal from measured results must be done.

How each stimulus signal responds to certain adverse measurement conditions and the benefits and drawbacks of some additional solutions are discussed. Signal length, number of averages and pre-emphasis all affect each signal's efficacy in the presence of noise pollution and time-variance. How each signal responds to non-linearity and the effect on signal-to-noise ratio is also discussed, as are each signal's theoretical ability to exploit bit depth or reject DC offsets.

Chapter 4 introduces a method of using long stimulus signals when taking measurements using a pulse reflectometry system. The theory behind the deconvolution is presented and

then verified with measurements from a pulse reflectometry system. The stimulus signals presented in Chapter 3 are then used to measure reflection functions from a waveguide model and are compared, with concentration on their immunity to added non-linearities, uncorrelated white noise and DC offsets.

Tests are then presented using waveguide models to measure the effect of the windowing of the reflection function that occurs in pulse reflectometry to simulate an anechoic termination. The effect of a discontinuity between the source tube and the object under test on measured reflections and calculated impedances is also discussed. Modelled results are then compared to results calculated from a pulse reflectometry setup and reflections from the source were integrated into the calculations to improve the results.

Chapter 5 presents object measurements using the pulse reflectometry setup, including a measure of viscothermal losses, the reflectance of the open end of the source tube and measurements of input impedance of mouthpieces. For the open end reflectance, this measurement is compared with the theoretically predicted value to judge the fitness of the pulse reflectometry setup.

Chapter 6 reviews the conclusions presented in the thesis. It summarizes the advantages and restrictions when using long stimulus signals and recommends the use of a slowly swept sine wave as a stimulus signal in most measurement scenarios. It also reviews the restrictions on the type of objects which can be measured using an acoustic pulse reflectometry system and reviews the actual measurements that were taken. Recommendations for further improving the measurement techniques and suggestions for new ways to measure objects are also given.

Chapter 2

Wind Instrument Impedance Measurement Techniques

Various measurements have been used to characterize the acoustical response of wind music instruments. These measures typically provide information about resonance frequencies that can be used to estimate intonation and response. Also, the time-domain impulse response of a system can be used to pinpoint and classify physical discontinuities along an air column. These results can be used to aid in the design of wind instruments and also to inform the interaction between instrument and player.

Wind instruments are usually modelled in systems theory as a basic two-port network of air pressure (p) and volume velocity (U) at both the input and output, as shown in Fig. 2.1. There are a number of acoustical measures that can be made of these systems, such as the pressure transfer function $T(f)$, the load impedance $Z_L(f)$ and the input impedance $Z_i(f)$, defined as:

$$T(f) = \frac{p_o(f)}{p_i(f)} \quad (2.1)$$

$$Z_L(f) = \frac{p_o(f)}{U_o(f)} \quad (2.2)$$

$$Z_i(f) = \frac{p_i(f)}{U_i(f)} \quad (2.3)$$

Early measurement techniques characterized the pressure transfer function, however measurements of output values are easily distorted by the shape and size of the measurement environment and ambient noise pollution. The input impedance is a more interesting and accurate acoustic measure because it is more immune to the effects of the measurement environment and because of the role it plays in the regeneration of sound at the lips (Benade, 1973).

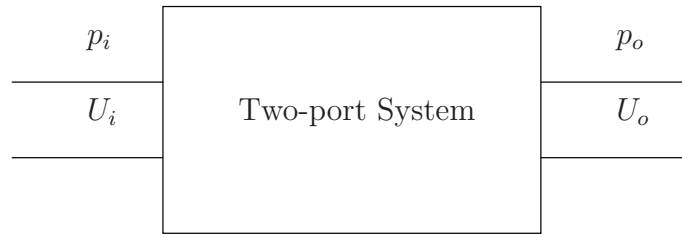


Figure 2.1 A basic two-port network.

There are a number of reviews on the subject of input impedance measurement for wind instruments (Benade and Ibis, 1987; Dalmont, 2001), however many reviews have concentrated on the use of multiple sensors that measure volume velocity either explicitly or in relation to pressure measurements. Recently there has been an increased use of pulse reflectometry, a single microphone measurement technique, to measure reflection functions of wind instruments (Watson and Bowsher, 1988; Keefe, 1996; Sharp, 1996; Buick et al., 2002).

Time-domain descriptions of acoustic systems are typically given by the impulse response, which is yielded by the inverse Fourier transform of the input impedance, and in the case of wind instrument acoustics corresponds to the response of the system with a closed entryway to a unit volume velocity impulse. This measure therefore includes many internal reflections within the instrument.

An alternate time-domain measure of an acoustic system is the reflection function, defined as the response of the air column when stimulated by a pressure impulse at the input which is anechoically terminated. This characteristic is significantly shorter in length, because signal energy traveling into the input disappears, rather than being reflected back into the system.

Pulse reflectometry setups measure the reflection function, which can be converted into its frequency-domain counterpart, a reflectance $R(f)$, which can be related to the input impedance by

$$Z_i(f) = Z_0 \frac{1 + R_i(f)}{1 - R_i(f)} \quad (2.4)$$

where Z_0 is characteristic impedance of the medium in the acoustic body over its length, defined as

$$Z_0 = \frac{\rho c}{S(x)} \quad (2.5)$$

where ρ is the air density, c is the speed of sound and $S(x)$ is a function for the cross sectional area of the cylinder. In the case of a straight cylindrical bore the function $S(x)$ can be replaced with the constant πa^2 , where a is the radius of the bore.

Reflection functions can also be converted into profiles of bore diameter using various layer-peeling techniques as described by Ware and Aki (1969) or Sondhi and Resnick (1983).

Most measurement methods presume that wave propagation is essentially one dimensional in the planar mode, ignoring higher order modes in the pipe. This means the measurements are valid only below the cut-on frequency of the first higher order mode, which in a cylindrical bore occurs at

$$f = \frac{1.84c}{2\pi a} \quad (2.6)$$

In all methods there is a calibration process, where the response of each of the sensors must be measured and stored for later deconvolution. Losses due to propagation can also be measured and deconvolved from the results. When comparing measurements and techniques it is also very important that the temperature remains constant between measurements, since minor variations in the speed of sound can have a large impact on measured results.

2.1 Volume Velocity Measurements

One major difficulty in measuring input impedance directly has been accurately measuring volume velocity. A review of the earliest impedance measurement techniques is given in Benade (1973) and Pratt et al. (1977), where techniques are described that avoid measuring volume velocity and instead keep it constant using a high impedance capillary feedback loop. Because the volume velocity will effectively be constant, only the pressure responses need to be measured at each frequency of interest.

However, there are difficulties keeping volume velocity constant. The sweep through the frequencies of interest must be done slowly to allow the feedback system to reach a state of equilibrium before a pressure measurement can take place. Environmental conditions can change over the course of the long measurements, making calibration difficult to maintain.

Also, because the system requires constant volume velocity, these techniques are also unable to measure how air flow affects the impedance, as will occur when the instrument is played.

Using a single sensor to measure air pressure and a single sensor to measure volume velocity is conceptually simple since both of the quantities needed to calculate the input impedance are measured directly. A number of early systems using this method are described in Pratt et al. (1977) and Elliot et al. (1982), where pressure and volume velocity probes are inserted into the mouthpiece of a wind instrument while a coupled loudspeaker is driven at a frequency that is stepped across the range of interest. The impedance can then be calculated from the ratio of the signals at the two probes.

Methods that measure volume velocity have the benefit that they can measure played instruments, since the body responds differently depending on the movement of air within it.

While pressure sensor measurements are robust and well developed because of the broad utility of microphones, there are no equivalent probes to directly measure particle and volume velocity. Most systems that measure volume velocity do so indirectly, such as a hot wire anemometer, which measures wind velocity in the plane perpendicular to the wire via temperature gradients.

While such systems are theoretically simple, the hot wire anemometer requires a lengthy and complicated calibration process and tends to be fragile. The volume velocity must be kept to within acceptable limits using a feedback control loop and synchronization issues and the presence of transients mean the excitation frequency must sometimes be swept very slowly, greatly increasing measurement times.

If the measurement time is long the temperature must be kept constant or else the resonances can drift over the frequency range. The measurement of volume velocity must also be corrected, since the anemometer only measures particle, not volume, velocity in the center, and viscosity at the walls causes the particle velocity to drop, meaning averages based on measurements at the center will overshoot the actual measure.

2.2 Multi-Microphone Methods

Instead of measuring the volume velocity directly, one can also use a pressure transducer that is proportional to the volume velocity thereby measuring it indirectly. Dalmont (2001) describes two methods in which a single pressure transducer signal is proportional to the volume velocity, either by mounting the microphone inside the stimulating loudspeaker enclosure or by attaching a relatively high impedance capillary tube between the speaker and the device under test and mounting a microphone there. These methods place a number of constraints on the physical apparatus used, but require very little computation to convert the measured values into impedance.

2.2.1 The Two-Microphone, Three-Calibration (TMTC) Technique

One of the primary techniques to measure impedance of acoustic devices since the late 1970s has been to use two pressure transducers spaced along a straight tube coupled to the system under study as shown in Fig. 2.2. Using two pressure sensors p_1 and p_2 , each placed at a distance L from a center point, we can relate the two measured pressures to the pressure (p_0) and volume velocity (U_0) at the midpoint between the sensors by:

$$\begin{pmatrix} \frac{(p_1+p_2)}{2} \\ \frac{(p_1-p_2)}{2} \end{pmatrix} = \begin{pmatrix} \cosh\Gamma L & 0 \\ 0 & Z_c \sinh\Gamma L \end{pmatrix} \begin{pmatrix} p_0 \\ U_0 \end{pmatrix}$$

where Γ is the propagation constant, dictating the magnitude and phase change of sound propagation in the air over the distance L .

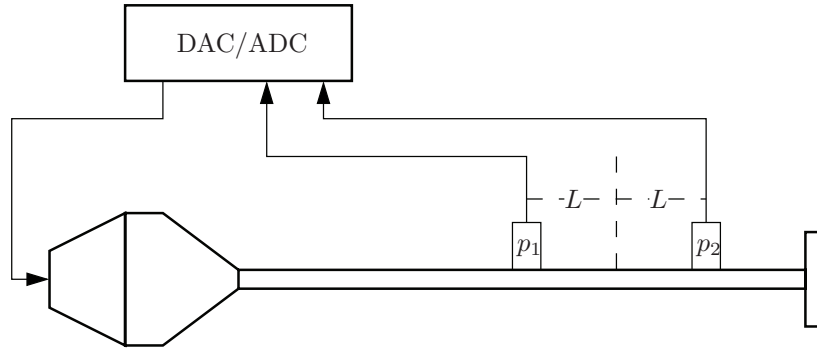


Figure 2.2 A two-microphone measurement apparatus.

Calibration of the variables can be done completely, in which the only assumption made of the measurement apparatus is that of linearity and stability of the system and these values are all set by measuring three predictable loads in what is called the Two Microphone Three Calibration (TMTC) method.

For a complete calibration, the three unknown variables have been set by measuring three test objects with losses that are accurately approximated by theory, usually closed cylinders of varying length. This method assumes accurate knowledge of the propagation constant, which can vary in measurement situations with air density, temperature and other conditions which are difficult to consistently reproduce.

2.2.2 Two Microphone Technique Variations

van Walstijn et al. (2005) describe a different method for calibrating a 2-microphone technique using 4-calibration steps, which does not depend on the calibration constant. This method assumes a frequency bandwidth limited by the higher-mode frequencies (a function of the duct-diameter), sufficient distance between the microphone and reference plane and linearity of the stimulating signal within the measurement duct.

Under these conditions, van Walstijn et al. (2005) relate the two pressure signals s_1 and s_2 to the pressure p and volume velocity U at the reference plane as:

$$\begin{pmatrix} s_1 \\ s_2 \end{pmatrix} = \begin{pmatrix} \alpha_1 & \beta_1 Z_c \\ \alpha_2 & \beta_2 Z_c \end{pmatrix} \begin{pmatrix} P \\ U \end{pmatrix}$$

and the ratio of the signals:

$$y = \frac{s_2}{s_1} = \frac{a_2 Z + \beta_2 Z_c}{a_1 Z + \beta_1 Z_c}$$

making the impedance:

$$Z = Z_c A \left(\frac{y - B}{y - C} \right)$$

where $A = -\beta_1/\alpha_1$, $B = \beta_2/\beta_1$ and $C = \alpha_2/\alpha_1$, which means the impedance can be deduced from the ratio of the microphone signals y and the three calibration parameters A , B and C . As with other methods, these parameters can be approximated, but at the cost of accuracy in the measurements.

The calibration uses four objects with accurately-predictable impedances: a zero-admittance termination and tubes of length L , $2L$ and $3L$ to measure the parameters A , B and C , which remain independent of the propagation constant Γ .

2.2.3 Errors

This method is subject to a number of measurement errors. Uncorrelated noise errors are manifest as inaccuracies at and around the singular frequencies related to microphone placement and calibration tube length. Calibration errors can occur if the impedance of the calibration objects are not correctly predicted, such as when the lengths of the objects are not accurately known and will also effect the impedance the most at the frequencies related to the distance between the microphones.

Errors will be concentrated when pressures on the two microphones are nearly equal in magnitude, at the frequency $f_m = c/2d$, where d is the distance between the microphones, and all of its integer multiples. This is because the signals will have mostly the same or opposite phase and thus ratio between the two provides little information. Singular frequencies also occur when the calibration tubes present zero impedance load, which occurs at $f_c = c/4L$ and all of its integer multiples.

Multiple pairs of microphones with varying spacing must be used to achieve a measurement over a wide frequency range, with calibration tubes of various length for each microphone spacing. A total calibration with three pairs of microphones requires a large number of different calibration tubes and measurements.

Signal levels must also be carefully monitored and chosen to achieve a good signal-to-noise ratio without creating non-linearities within the source tube or instrument. All of these calibration data assume a constant propagation constant and measurement conditions such as temperature and air density must be as consistent as possible.

When choosing a stimulating signal in these techniques, the primary concern is that sufficient energy is excited across the frequency range. However, it is important to drive the system linearly, since these measurement techniques assume the signal propagates linearly through the apparatus and that the sensors are linearly related to pressure. To this end, it is advantageous to use a method that will clearly illustrate when non-linear distortion occurs in the signal.

2.3 Single-Microphone Methods

As previously mentioned, it is also possible to determine the input impedance from a measured reflection function, requiring only a single pressure measurement. The technique

of pulse reflectometry has a long history, and was initially used in geophysical applications with large explosive charges causing seismic disturbances. The impedance mismatch at each layer of the Earth's depth would reflect back a certain amount of the energy and the time delay and smearing of the reflection could be measured to infer both the depth and composition of each successive layer.

Throughout the 1970s this technique was adapted by Sondhi and Gopinath (1971) and others to use spark discharges fed through a source tube to describe airway dimensions, first on dogs (Jackson et al., 1977) and then on people (Fredberg et al., 1980), with the hope to compare favorably with measurements made using X-rays.

Benade and Smith (1981) describe a pulse reflectometry measurement system for wind instrument measurements as early as 1966, primarily for analysis of the group and phase repetition times within instrument bodies. FFT developments in the early 80s meant the same apparatus could then be used to calculate input impedance functions and preliminary results of tube impedances measured by inserting a microphone directly into the mouthpiece of wind instruments were presented.

Watson and Bowsher (1988) describe using pulse reflectometry to find acoustic and structural properties of wind instruments, mapping the inside of the wind instrument, since the pulse is reflected back at impedance mismatches within the instrument that typically arise at valves and diameter variations.

These measurement techniques use a single pressure transducer and have the advantage of directly measuring the impulse response of an instrument in the time-domain. Although the time-domain input impulse response and reflection functions are related to the input impedance and can be derived from it, these relations may be limited by frequency response issues-

2.3.1 Measurement Setup

The apparatus for pulse reflectometry consists of a source, usually realized as a loudspeaker, and a pressure transducer, usually a microphone, attached to a long "source" tube as shown in Fig. 2.3. The source is coupled to one end of the tube at a length L_{S-M} away from the microphone, making the round trip travel time $T_{S-M} = 2L_{S-M}/c$. The microphone is embedded flush in the wall of the source tube at a distance L_{M-O} from the object, resulting in a roundtrip object-to-microphone travel time of $T_{M-O} = 2L_{M-O}/c$. The overall length of the tube is thus $L_{S-M} + L_{M-O}$ and the total round trip travel time $(2L_{S-M} + 2L_{M-O})/c$.

If we assume the source is a pulse of short duration, we define $f(t)$ as the pulse that passes by the microphone at time $t = 0$ and set $r_s(t)$ as the reflection response of the source, including propagation and wall losses over the distance L_{S-M} . $r_o(t)$ is the reflection function of the object attached to the other end of the tube, including propagation and wall losses over the distance L_{M-O} .

The microphone signal $s(t)$ will be first the incident pulse going right, followed after a time of T_{M-O} by the left-traveling first object reflection. This object reflection will be the

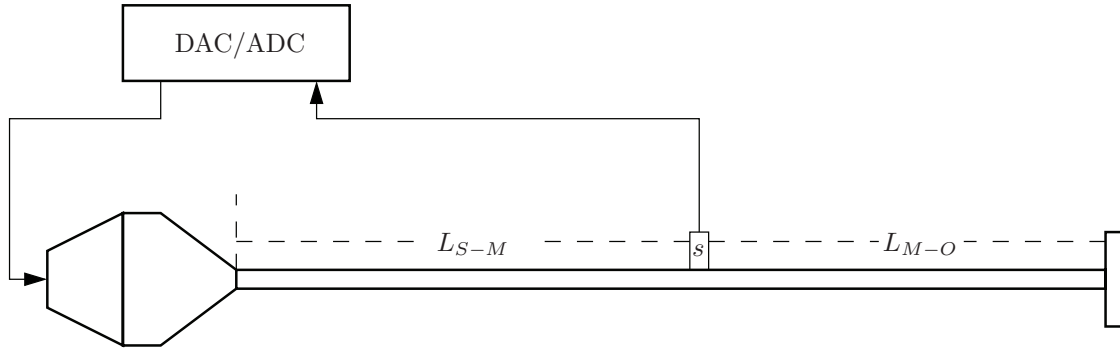


Figure 2.3 A pulse reflectometry apparatus.

object reflectance convolved with the pulse shape. That object reflection will return again after it has again reflected back from the source after a time of T_{S-M} , continuing until the signal dies away. This gives us an infinite sum for the microphone signal as:

$$\begin{aligned}
 s(t) = & f(t) + f(t) * r_o(t) * \delta(t - T_{M-O}) + \\
 & f(t) * r_o(t) * r_s(t) * \delta(t - (T_{M-O} + T_{S-M})) + \\
 & f(t) * r_o(t) * r_s(t) * r_o(t) * \delta(t - (2T_{M-O} + T_{S-M})) + \dots \quad (2.7)
 \end{aligned}$$

where δ is the Dirac delta defined as $\delta(x - T) = \text{inf}$ when $x = T$ and 0 otherwise, operating as a delay of time T .

In existing literature a short pulse is sent from the driver and the reflection from the system is measured after a travel time of $(L_{S-M} + 2L_{M-O})/c$. The first $2L_{S-M}/c$ ms of the response of the system can then be measured before reflections back from the driver reappear at the microphone. This limits the types of systems to be measured to have reflectances shorter than $2L_{S-M}/c$ ms.

The response at the input to an impulse with a non-reflecting source (i.e. a semi-infinite tube attached to the input) is $p(t) = \delta(t) + r(t)$, where $r(t)$ is the measured reflection function and $Z_0 u(t) = \delta(t) - r(t)$. For a totally reflecting source (i.e. with a closed input) the input impulse response is $p(t) = \delta(t) + r(t)$ and $Z_0 u(t) = \delta(t)$.

Most pulse reflectometry simulates a non-reflecting source by increasing L_{S-M} so that the reflection function will die out to the noise floor level before source reflections return after T_{S-M} , in which case windowing simulates a non-reflecting source where $r_s(t) = 0$. There is a practical limit to this technique, as high frequency components are severely attenuated as the pipe length increases, making the measured reflectance at high frequencies unreliable (Sharp, 1996).

The pulse reflectometry setup described in the rest of this section will assume a non-reflecting source, such that the reflectances measured are sufficiently small that source reflections can be windowed out. Other methods of working with a reflecting source are

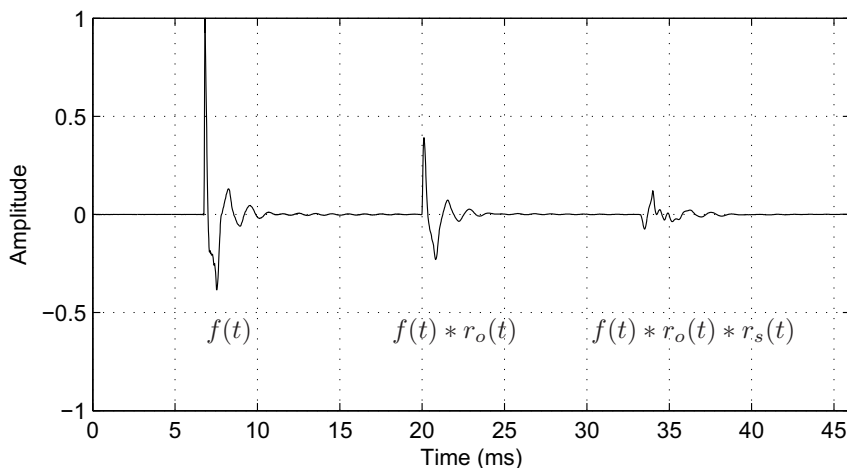


Figure 2.4 The calibration measurement for a pulse reflectometry system showing $f(t)$, $f(t) * r_o(t)$ and $f(t) * r_o(t) * r_s(t)$.

described in Section 2.3.4 and a novel method of including source reflections is described in Section 4.1.

2.3.2 System Calibration

A partial calibration can be done simultaneously along with the measurement, as long as $f(t)$ is less than T_{M-O} and an adequate model of viscothermal and propagation losses can be included. However a calibration measurement using an infinite impedance termination on the end will allow measurement of $f(t)$ and all of the viscothermal losses over T_{M-O} , so the calibration step is helpful.

The calibration step measures the pulse that will enter the system by closing the end of the source tube with a rigid cap that has a theoretical impedance of infinity at all frequencies. This allows the effect of the driver, microphone and viscothermal losses along the tube to be deconvolved out of the instrument measurement. The infinite impedance reflector has a pressure reflection function of 1, so the second pulse passing by the microphone in a calibration step will be able to measure $f(t)$ plus the effect of losses over T_{M-O} .

This measured pulse response $r_{pulse}(t)$ will be deconvolved out of the instrument response, eliminating the effect of the interface, driver and microphone responses and viscothermal and propagation losses. We will also see in Section 4.2 that measurements from this step can help deconvolve some of the source reflections.

2.3.3 Measurement Procedure

A device can be coupled to the end of the reflectometry setup, and a measurement r_{meas} can then be taken. Time windows must be applied to eliminate source reflections so the measurement corresponds to a reflection function. The effects of the source, microphone and viscothermal losses can then deconvolved out of the measurement, leaving the frequency-domain reflectance of the system as:

$$R_{inst}(f) = \frac{FFT(r_{meas}(t))}{FFT(r_{pulse}(t))}$$

This can be converted back to the time domain by an IFFT, yielding the reflection function of the instrument. Because of propagation within the tube, high frequency energy in the signals will be attenuated over distances, meaning reflectance measurements are highly susceptible to errors at those frequencies. Windowing before conversion back to the time domain can yield cleaner responses, although care must be taken when modifying low-frequency information, as this can drastically distort the time-domain signal.

2.3.4 Measuring Long Reflectances

Reflection function length is limited by the travel time T_{S-M} after which time reflections from the source will return to the microphone and if the source tube is too short or the reflection function of the object under test is too long, this will be before the reflection function dies away.

The obvious solution of increasing the length of the tube creates problems, since the increased losses to the walls and air result in poor responses at high frequencies. A number of papers have concentrated on refinements of this technique for measuring longer objects. Marshall (1992) suggests a different approach to measurement allowing arbitrarily long objects to be measured.

His technique involves placing the microphone at the very end of the source tube. Two calibration steps are needed: one simulates an anechoic termination at the end by attaching a tube of sufficient length to measure the pulse shape and another simulates an infinite impedance termination by affixing a rigid cap to measure the reflection function of the driver.

He reduces the infinite sum of the pressure signal in Eq. 2.7 to

$$S(f) = \frac{F(f)(1 + R_o(f)e^{-jfT_{M-O}})}{1 - R_o(f)R_s(f)e^{-jf(T_{M-O} + T_{S-M})}}$$

in the frequency domain. $F(f)$ and $R_s(f)$ are determined using the calibration stages, and thus the reflectance of the object under test R_o can be calculated from the entire measured pressure signal, without the constraint of a non-reflecting source.

Bore reconstructions presented in the paper are correct at greater axial distances than those made previously, but the profiles can be erratic. Keefe (1996) presents a similar technique of taking the sum of the reflections with the measurement apparatus inserted directly into the body of the instrument.

Sharp (1996) eschewed this method because of poor results and tried to actively cancel the reflections from the driver by stimulating it using an out-of-phase copy of the reflection function at an appropriate time delay, however there are still errors present in the reconstructed profiles at these locations.

The effect of source reflections on reflection function measurements has focussed on the length of bores that can be reconstructed using a given source tube size, without concentration on the effect of simulating a non-reflecting source on measured input impedance. Integration of source reflections and their effect on input impedance measurements is discussed in Chapter 4.

2.3.5 Stimulus Length

Current pulse reflectometry setups limit their stimulus signals so that the measured pulse signal $f(t)$ will be shorter than the round trip microphone-to-object travel time T_{M-O} , usually using some type of band-limited noise or filtered impulse as in Sharp (1996) and Keefe (1996). Improvements to standard pulse reflectometry described in Chapter 4 do away with this requirement, making a number of stimulus signals used to characterize impulse responses available in pulse reflectometry.

These methods are therefore reviewed in the next chapter, with concentration on their efficacy and applicability in wind instrument pulse reflectometry measurements and their resistances to situations of non-linearity, time-invariance or noise pollution.

2.4 Apparatus Issues

Multiple- and single-microphone methods both couple the device under test to the end of a cylindrical tube. If the diameters of the tube and device are not equal there will be an impedance mismatch at the junction, distorting the impedances calculated by each method. Pagneux et al. (1996) shows that in multiple-microphone measurements this distortion is caused by excitation of higher modes at the discontinuity, resulting in a constant dB offset between the calculated and real impedances.

The most substantial effect of this mismatch on impedances calculated from a single-microphone method is also a constant dB offset, however the impedance mismatch also greatly increases the length of the reflection function. As the pressure wave from the device under test passes back into the source tube it will be partly reflected back into the device, exciting it again. Models used in Section 4.2 show that windowing these longer reflection functions, as is necessary in pulse reflectometry setups, introduces more complicated distortions to the calculated impedances.

To improve measurement accuracy the measurement apparatus diameter should closely match the diameter of the object under test whenever possible. One can correct some of the distortion by subtracting a constant offset, but in acoustic pulse reflectometry measurements this will not fully eliminate distortion.

An alternative to using multiple source tubes is to use a set of adapters that taper from the tube to the device opening slowly, minimizing impedance mismatches and reducing distortion. If this method is used, appropriate couplers must be used for all device and calibration measurements.

Chapter 3

Stimulus Signals for Acoustic Measurements

There is a great deal of literature available on impulse-response measurement techniques for capturing room acoustics, including descriptions of various techniques (Rife, 1989; Griesinger, 1992; Farina, 2000) and reviews (Müller and Massarani, 2001; Stan et al., 2002).

These discussions mainly focus on how effective each stimulus signal is for measuring room impulse responses, but there are different considerations when using these techniques to measure wind instrument reflection functions. This chapter reviews signal properties given in the literature, while the next chapter discusses the efficacy of each signal type for reflection function measurements in a pulse reflectometry system.

The response of a linear, time-invariant, discrete-time system to an impulse $\delta(t)$ completely characterizes the system response and is defined as:

$$h(t) = \sum_{k=-\infty}^{\infty} \delta(t)h(t-k)$$

If we test the system with an input function $x(t)$ the result of convolving $x(t)$ with the impulse response $h(t)$ will be the output signal $y(t)$:

$$y(t) = h(t) * x(t) = \sum_{k=-\infty}^{\infty} x(t-k)h(k)$$

For time-domain signals, convolution with long impulse responses can be computationally intensive in the time-domain because of the large number of required multiplications. If the signals are converted to the frequency-domain the convolution operation becomes a simple multiplication of the two responses:

$$Y(f) = H(f)X(F)$$

This is useful when measuring impulse responses, since we can test the system with a long, high-energy input function $x(t)$ and recover the impulse response $h(t)$ by dividing in the frequency domain:

$$H(f) = \frac{Y(f)}{X(f)}$$

Because frequency-domain deconvolution involves division by the stimulus signal, it is important that this signal has sufficient energy at all relevant frequencies to avoid division by a zero or near zero value. If high- and low-frequency energy is not present in the stimulus signal, these values should be excluded from the division operation, otherwise time-domain representations of impulse response can be heavily distorted.

As will be discussed in Chapter 4, we can drive a pulse reflectometry system with a complex input signal and deconvolve it from the response to get the system impulse response. The impulse response of the pulse reflectometry system is the response of the microphone to a stimulus applied at the speaker, as described by Eq. 2.7, which must be processed, say by windowing, to yield a reflection function for the object under test.

Chapter 4 includes a comparison of each stimulus type's ability to reproduce input impedances that are calculated from measured reflection functions, while the review of stimulus signal types that follows describes each signal's fitness when measuring impulse responses.

3.1 Impulses and Periodic Pulses

Theoretically the simplest type of stimulus signal, digital impulses are just single samples of maximum amplitude followed by all zeros. When testing using impulses, no deconvolution or processing needs to take place, as the measured response is theoretically exactly the impulse response of the system. Realizing a pure impulse acoustically is impossible, however, and a stretched pulse will actually be emitted instead.

While impulses are straightforward and easy to implement, the energy in the signal is very limited because the ratio of peak to average power is very high. This lack of stimulating energy makes it very difficult to achieve good signal-to-noise ratios in pure impulse measurements, since they are extremely susceptible to noise pollution. Short, loud impulsive noises are especially destructive, as they are usually very similar to the impulse itself and thus give rise to simple echoes of the impulse response.

To reduce the background noise and increase the signal-to-noise ratio, multiple averages of the impulse response measurement can be taken, as in periodic pulse testing. A regularly repeated pulse is input to the system and the response is averaged over a number of periods to diminish background noise and improve the signal-to-noise ratio. When using periodic testing the measured response is actually the periodic impulse response $h'(n)$, which relates

the periodic input $x'(n)$ to the periodic output $y'(n)$ by:

$$y'(t) = \sum_{k=0}^{L-1} x'(k)h'(n-k)$$

with a period of L . ($n-k$) is evaluated modulo L .

The periodic-impulse response $h'(n)$ is similar to the impulse response $h(n)$, except it is convolved with the periodic impulse. This means that if the real impulse response is shorter than the measurement period length the end of the regular response will overlap the beginning of the measured periodic response. This is often referred to as time aliasing and when using any periodic impulse response measurement it should be avoided by choosing the period of the test signal to be longer than the impulse response being measured.

3.2 Maximum Length Sequences (MLSs)

Maximum Length Sequences (MLSs) are similar to periodic pulse testing, although they increase the amount of energy being put into the system because of their extremely high signal-to-peak ratio. MLSs, or pseudo-random binary signals, are periodic two-level sequences of length $L = 2^N - 1$, where N is an integer, which contains near-equal energy at all frequencies.

Because the signals are constructed entirely of samples which are either 1 or -1, the signal has the lowest peak-to-signal ratio and will deliver a lot of energy to the system, increasing the signal-to-noise ratio of measurements. Since MLSs measure the periodic impulse response, it is again important that the impulse response to be measured be shorter than the MLS period L .

Recovering the impulse response from MLS testing is slightly different than when using other methods. The impulse response of a system is found by cross-correlating the input MLS and the system output because the auto-correlation of an MLS is similar to an impulse. The auto-correlation function of an MLS of length L (with the states chosen to be the values +1 and -1) is $\phi_{xx}(n)$, defined as:

$$\begin{aligned} \phi_{xx}(n) &= x'(n)\phi x'(n) \\ &= \frac{1}{L} \sum_{k=0}^{(L-1)} x(k)x(k+n) \end{aligned}$$

or

$$\begin{aligned} \phi_{xx}(n) &= \frac{-1}{L} \text{ for } 0 < n < L \text{ and} \\ \phi_{xx}(0) &= 1 \end{aligned}$$

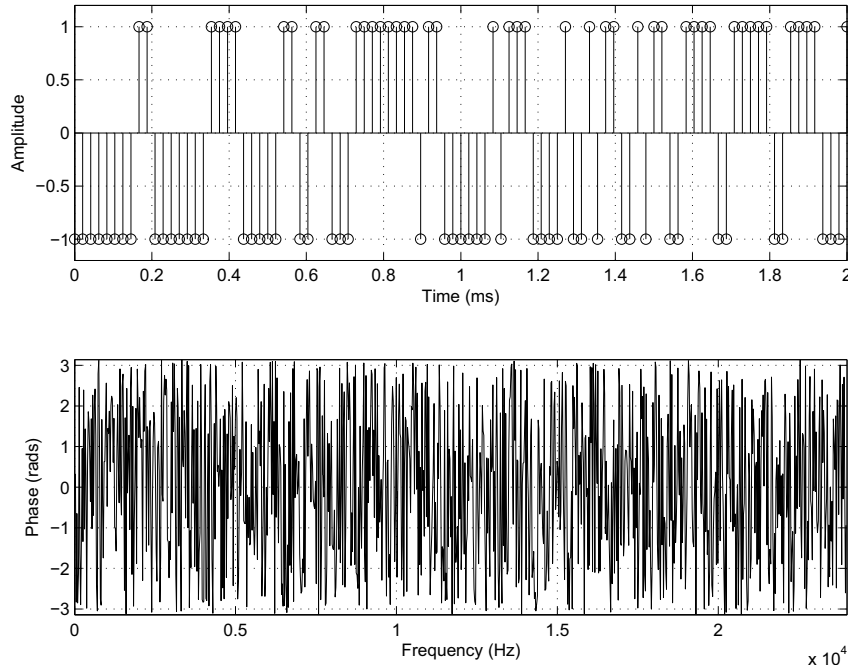


Figure 3.1 Time-domain signal and frequency-domain phase information for a Maximum Length Sequence (MLS).

In other words, the auto-correlation function of an MLS is 1 at zero lag and $-1/L$ for all other lags. As N increases, the auto-correlation function approaches the ideal function, 1 for zero shift and zero for all others.

To measure the impulse response of a system the MLS is applied to a linear system and the response is sampled and then cross-correlated with the original sequence, yielding a result close to the impulse response. When applied to a linear time-invariant system with periodic impulse response $h'(n)$, the system output $y'(n)$ is:

$$y'(n) = x'(n) * h'(n) = \sum_{k=0}^{L-1} x'(k)h'(n - k)$$

To find the periodic impulse response $h'(n)$, $y'(n)$ is cross-correlated with $s'(n)$:

$$\begin{aligned} \Omega_{xy}(n) &= x'(n)\phi y'(n) \\ &= x'(n)\phi(x'(n) * h'(n)) \\ &= (x'(n)\phi x'(n)) * h'(n) \\ &= \Omega_{xx}(n) * h'(n) \end{aligned}$$

and thus the periodic cross-correlation of output with input is equal to the convolution of the auto-correlation with the periodic impulse response.

The power delivered by an MLS is 2^N times more than a simple periodic unit sample with a similar flat response. This is because an MLS has a scattered phase spectrum, distributing energy for different phases over a long period of time.

The frequency spectrum of an MLS signal will generally have equal energy in all frequency ranges, with a randomized phase spectrum as can be seen in Fig. 3.1, showing that an MLS is very similar to an impulse, but instead of having each frequency component being coincident, as is the case with the impulse, each frequency component is randomly distributed over time. When the measurement experiences uncorrelated impulsive noise this phase randomization will distribute the noise evenly throughout the measured response, minimizing the concentration of the distortion in one time or frequency range.

One reason MLSs have historically been popular is because of their simplicity of generation. A generator can be implemented using a binary shift register of length N (Davies, 1966) with added exclusive-or gates, sometimes referred to as taps, which were connected back to the register. For a register length of N stages there are a maximum of 2^N possible states and sequences generated from this shift register can be divided into maximum and non-maximum length sequences, where an MLS will cycle through all $2^N - 1$ possible states before repeating. Note the state of all zeros will never vary because feedback is performed using exclusive-or gates.

A number of tap positions for MLS generators exist which must meet the conditions that the characteristic polynomial of the register is irreducible and primitive, so the sequences do not repeat before encountering the $2^N - 1$ states. This behaviour is also easily implemented in software with the use of tables of tap positions.

MLS measurements are usually done first by stabilizing the system by playing the MLS initially to "prime" the system and then repeating it, making the minimum system measurement time $2L$. In practice the signal can be repeated many times with all responses after the first being averaged together, which often happens in hardware MLS systems, where a fixed number of bits in the shift register mean that the period time is inflexible and the only way to increase the signal to noise ratio is to increase the number of averages.

Averaging can be applied to the MLS measurement technique to increase the noise immunity, where multiple measurements are taken with the same stimulus and then averaged together to reduce the effects of uncorrelated noise pollution on the measurement.

3.3 Golay Codes

Golay codes are similar to MLSs, in that they are both two-level sequences where the impulse response of the system under test is found using auto-correlation. However, instead of having one stimulus whose autocorrelation is an impulse, Golay codes are a set of two signals A and B generated such that the sum of the auto-correlations of the signals is an

impulse.

As described by Foster (1986), Golay codes can be used to measure the impulse response of a system by probing the system with the first code and correlating the response with that code, repeating with the second code and summing the result of those correlations.

The two sequences $a(n)$ and $b(n)$ are defined as a Golay pair of length L if

$$\begin{aligned}\phi_{aa}(0) + \phi_{bb}(0) &= \sum_{k=0}^{L-1} [(a(k)a(k+n) + b(k)b(k+n))] = 2L \\ \phi_{aa}(n) + \phi_{bb}(n) &= 0 \text{ otherwise}\end{aligned}\tag{3.1}$$

The results of probing the system with the first code is $y_a(t) = h(t) * a(t)$ which is then correlated with the original sequence, yielding:

$$\begin{aligned}\phi_{ya}(n) &= \sum_k a(k)y(k+n) \\ &= \sum_j h(j) \sum_k a(k-n)a(k-j)\end{aligned}$$

We can derive $\phi_{yb}(n)$ similarly.

Summing the correlations yields:

$$\phi_{ya}(n) + \phi_{yb}(n) = \sum_j h(j) \sum_k [a(k-n) + b(k-n)b(k-j)]$$

and since a and b are a Golay pair, we can use Eq. 3.1. The sum over k equals zero, except when $n = j$ where it is $2L$ and therefore the sum of the correlations is $2Lh(n)$, the impulse response scaled.

Any uncorrelated noise in the measurements is attenuated by the amount the impulse response is scaled, and thus the signal-to-noise ratio for Golay codes when compared to a single impulse is $10\log(2L)$ (Zhou et al., 1992).

Given a pair of Golay codes each of length L , it is simple to create a pair of Golay codes of length $2L$ using the appendix method. Starting with an initial pair of Golay codes a_1 and b_1 :

$$\begin{aligned}a_1 &= \{+1 \ +1\} \\ b_1 &= \{+1 \ -1\}\end{aligned}$$

we can create another pair of codes by appending the two previous ones, such that:

$$\begin{aligned}a_{n+1} &= \{a_1 \ b_1\} \\ b_{n+1} &= \{a_1 \ -b_1\}\end{aligned}$$

While similar to MLSs, Golay codes benefit from being length 2^N sequences instead of $2^N - 1$, making FFT techniques more efficient, and from a simplified construction scheme.

They can also be used without circular auto-correlation, allowing non-periodic probing and measurement of impulse responses longer than the code. However, since the response of the system to two separate codes needs to be measured, the energy delivered to the system is much lower compared to MLSs requiring equal measurement time.

3.4 Frequency-Domain Designed Noise

In the frequency domain, MLSs and Golay codes have a predominantly flat frequency component, while the phase is randomized. While these two signal types are generated in the time domain, it is possible to design a signal with similar frequency-domain characteristics in the frequency domain allowing signals of arbitrary length to be constructed. Frequency-domain designed noise can be used as an impulse response measure, where frequency-domain functions for magnitude emphasis and a randomized phase can be converted back to a time domain test signal.

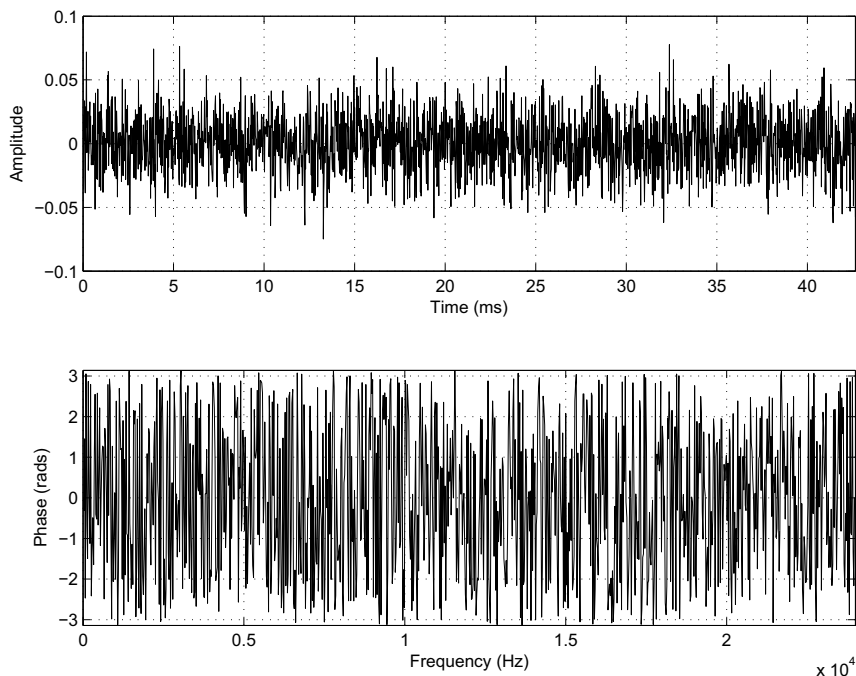


Figure 3.2 Time-domain signal and frequency-domain phase information for a designed random noise signal.

This designed noise can be made at any signal length, although for increased processing speed, it is most beneficial for the length to be a power of 2. While this increases computation efficiency, the time-domain signal is generally not binary, and so does not maximize

the peak-to-signal ratio, as MLSs and Golay codes do. A number of older impulse response measurement systems use periodic windows of noise, say of 1024 samples, which are then deconvolved out of the response in the frequency domain. These FFT analyzers have many properties in common with periodic noise testing, although the deconvolution procedure is somewhat different.

3.5 Swept Sines

Swept sines (or chirps) are constructed using a basic sine function, where the frequency is varied across the frequency spectrum of interest using a sweep function $f(t)$:

$$x(t) = \sin(f(t))$$

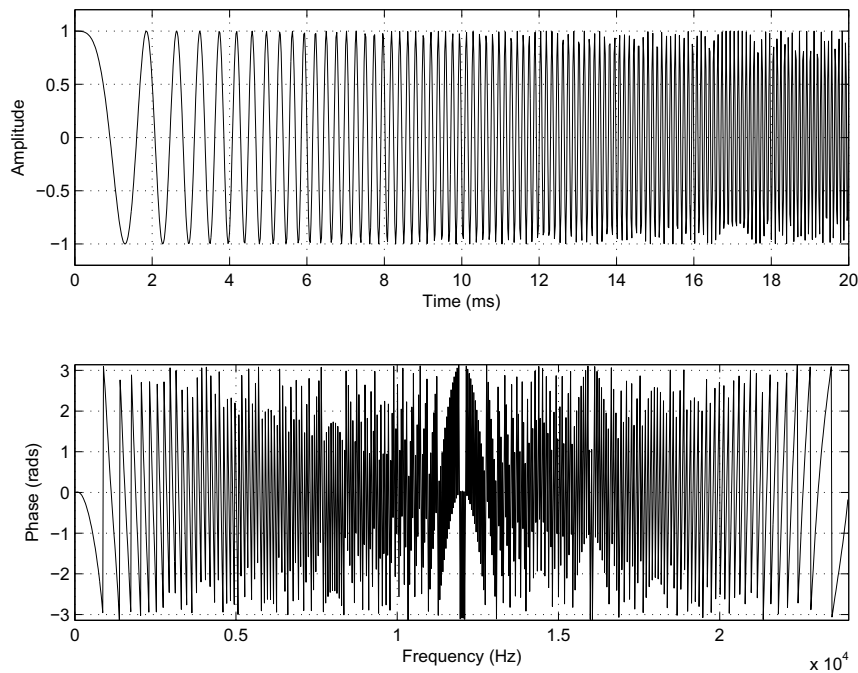


Figure 3.3 Time-domain signal and frequency-domain phase information for a linearly swept sine.

Signals discussed thus far have had the general properties of noise, where the frequency-domain magnitude is constant and the phase is randomized. Sine sweeps have a frequency-domain representation weighted depending on the trajectory of the sweep. The most common choices, linear and logarithmic sweeps, result in monotonic phase and either even or low-frequency emphasized magnitude.

The instantaneous frequency of the generating function is the derivative of $f(t)$ and thus if we want it to linearly vary between two frequencies ω_1 and ω_2 over a time T , we will set:

$$\frac{d(f(t))}{dt} = \omega_1 + \frac{(\omega_2 - \omega_1)t}{T}$$

which means

$$f(t) = \omega_1 t + \omega_1 + \frac{(\omega_2 - \omega_1)t^2}{2T}$$

To generate a sweep that varies logarithmically between the two frequencies over the time, we can likewise set:

$$f(t) = \frac{\omega_1 T}{\ln(\frac{\omega_2}{\omega_1})} (e^{\frac{t}{T} \ln(\frac{\omega_2}{\omega_1})} - 1)$$

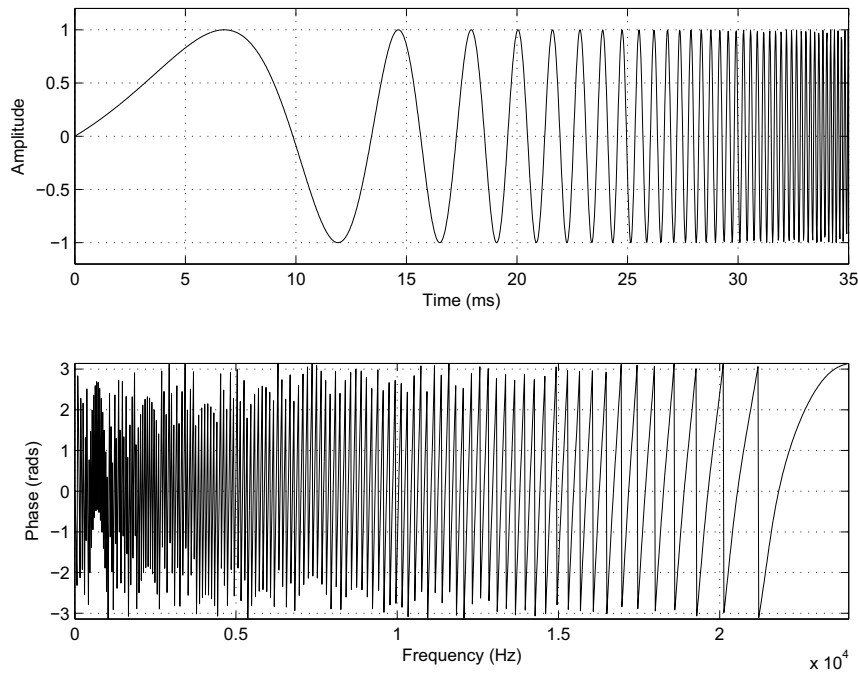


Figure 3.4 Time-domain signal and frequency-domain phase information for a logarithmically swept sine.

Sweeps performed over a longer period of time will contain more energy and therefore the length of the sweep directly affects the signal-to-noise ratio of the measurement. The ability to specify the sweep function means that certain frequency ranges can be emphasized by allowing the function to spend more time on those frequencies.

The most important aspect of swept sines for impulse response measurement is that the deconvolution process can separate non-linear distortion from linear system response. It is easiest to see how this occurs when deconvolving using a linear filter. Deconvolution of the swept sine can be done with frequency-domain division or by using a time-reversed version of the sine itself as the impulse response for a deconvolving filter. The deconvolution filter delays frequency components so that non-linear distortion is separated in time from the linear response. Farina (2000) finds that with a logarithmic sweep the time delay Δt between an instantaneous frequency and N times it is:

$$\Delta t = T \frac{\ln(N)}{\ln\left(\frac{\omega_2}{\omega_1}\right)} \quad (3.2)$$

showing the time at which each harmonic order can be found. Since Δt increases with $\ln(N)$, the higher orders will be less spaced than lower ones, overlapping unless T is sufficiently large.

Both logarithmic and linear sweeps push harmonic distortion out of the linear response, so measuring the linear response using a logarithmically swept sine will only increase the signal-to-noise ratio at low frequencies at the expense of high frequency resolution. If the sine sweep is logarithmic, however, the harmonic distortion will be spaced according to Eq. 3.2 and if the sweep length is slow enough, non-linear responses at different harmonic orders can be separated and measured. In a linear sweep these responses occur concurrently and are inseparable.

3.6 All-Pass Sequences

All-pass sequences are created by feeding an impulse through a series of all-pass filters to stretch it over time by changing the phase component of the signal. This can increase the amount of energy present in the signal by decreasing the peak value, allowing for a sizable decrease in the peak-to-signal ratio and therefore an increase in the signal-to-noise ratio of measurements.

All-pass sequences resemble other time stretched pulse methods in their applicability. They are very good at taking quick measurements from a device, because of their short signal length, which is helpful when trying to characterize the time variance of a system. They can also be easily designed to match frequency response characteristics using spectral warping and other filter design methods that are well developed.

Griesinger (1992) describes a method using an impulse as input to an available artificial reverberation unit and using the output of that as the stimulus signal for an impulse response measurement. Deconvolution on the signal measured using an all-pass sequence is very elegant and simple, involving time-reversing the measured response and feeding it back through the same all-pass network. It is also possible to time-reverse the stimulating

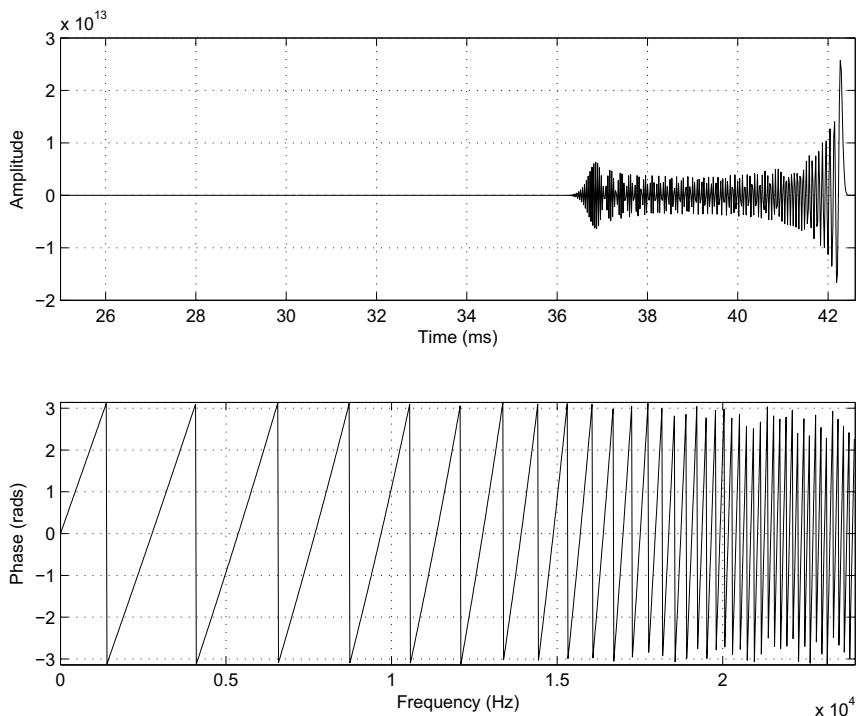


Figure 3.5 The time-domain signal and frequency-domain magnitude and phase information for an All-Pass Sequence.

signal before taking the measurements instead, allowing one to simply feed the measured signal back into the all-pass network as is.

It is also possible to smooth the time-domain envelope of the all-pass sequence, maximizing dynamic range of the stimulus signal, with an invertible filter (Abel and Berners, 2004). The design of the all-pass delay network also greatly affects the phase characteristics of the resulting stimulus signal and existing methods for all-pass filter design, such as Abel and Smith (2006) can be used to design the network. One of the drawbacks of this signal type is how hard it is to predict the stimulus length because of the complex relationship between pole-zero placement and the stretching of the pulse.

3.7 Time Stretched Pulses

Stretched impulses can also be designed in the frequency domain by specifying a varying phase function and converting back to the time-domain. Aoshima (1981) describes how to create a stretched impulse by specifying a frequency domain phase function with a user specified amount of stretching. The Aoshima Time Stretched Pulse is then converted to

become a high energy time-domain signal.

Improvements on this technique and a synthesis method are given in Suzuki et al. (1995), which describes an Optimized Aoshima Time Stretched Pulse (OATSP) that can measure of longer impulse responses, at frequencies all the way up to the Nyquist frequency.

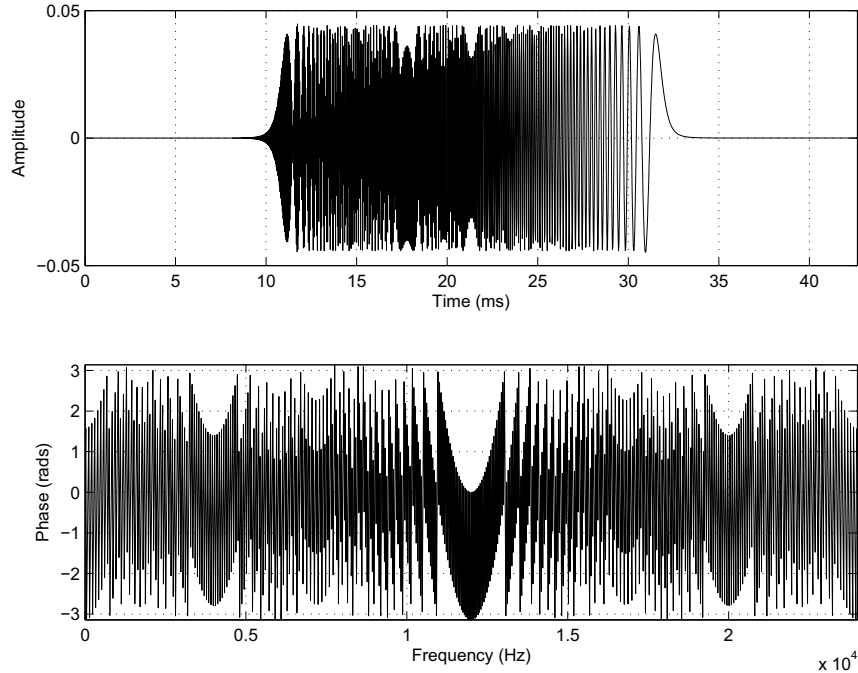


Figure 3.6 Time-domain signal and frequency-domain phase information for an Optimized Aoshima Time Stretched Pulse (OATSP).

OATSPs are designed with the first half of their frequency response as:

$$H(f) = e^{j4m\pi f^2/N^2}$$

and the second half as a mirror image of the first half. Here m is an integer determining how stretched the OATSP will be in the time domain, and should be verified so it does not produce any sudden discontinuities. Setting $m = N/4$ usually results in a signal with smooth attack and decay that can be used for impulse response testing.

In the way that OATSPs attempt to stretch the phase components of an impulse over time, they are similar to sine sweeps and all-pass sequences, however, some aspects of the design like the stretching factor and the frequency-domain design make it less flexible than swept sines.

3.8 Refinements and Comparisons

The signals presented can, and in many cases should, be processed and used differently, depending on the measurement situation. They can be refined to provide increased overall signal-to-noise ratio or greater accuracy in certain frequency ranges. The methods are also affected differently by various degradations to the signal and therefore the measurement environment will influence which signal is most appropriate.

3.8.1 Averaging

With any signal type multiple results can be averaged into a single response, minimizing the effect of uncorrelated background noise and increasing the effective signal-to-noise ratio of the measurement. Each doubling of the number of averages taken will decrease the level of uncorrelated white noise by 3 dB.

One of the main disadvantages of averaging is how the response changes in the presence of time-variance. If the system is not perfectly time-invariant, averaging will reject parts of the actual system response which vary and the signal-to-noise ratio gain could be offset by the loss of parts of the impulse response. Care should be taken when measurement conditions vary and in wind instrument measurements which use a large apparatus it can be difficult for the temperature to be maintained around the device.

It is known that MLSs are susceptible to errors when measuring time-variant systems (Svensson and Nielsen, 1999), both when large numbers of averages are used and when they are not, especially in the case of measurements performed in non-anechoic laboratory environments. Golay codes are also sensitive to time-variance, since measurements using both codes of the pair are necessary and cannot be performed simultaneously.

Methods requiring averaging to achieve good signal to noise ratios have a distinct disadvantage compared to more flexible single measurement techniques such as the swept sine methods or frequency-domain designed noise or chirps. These techniques can avoid multiple averages, yielding better signal-to-noise ratios simply by using longer stimuli, which ensure time-variant parts of the linear response are still included. In pulse reflectometry, this may be important as measurement conditions will change over long times, and thus the system could be said to be time-variant.

3.8.2 Pre-emphasis

Many of the signal types discussed go through an invertible pre-emphasis phase to increase signal energy in specific frequency ranges of the stimulus signal. Often when taking acoustical measurements, a specific range of the frequency response is the most interesting, so the stimulus signal is pre-filtered to concentrate energy there. This is often done when shorter stimulus signals, which can deliver limited energy to the system, are required.

Rife (1989) gives a comparison of pre-emphasis techniques in MLS and Time Delay Spectroscopy, a method of individual sine testing, where an invertible filter is used on the stimulating signal to boost signal energy at that region and using the inverse filter on the measured response. This type of emphasis benefits the MLS and noise techniques over other methods, however newer swept sine methods which use digital deconvolution do not require a similar pre-emphasizing filter. Swept sines can be emphasized by designing a custom path across the frequency range of interest instead of using a filter to boost the level. Since the function will cause the sweep to spend more time on certain frequency ranges, the signal to noise ratio at these points will be increased also.

With All-Pass sequences, since pole placement will effect the amount of time the stimulus will linger in a certain frequency range, the placement of those poles is similar to the design of the frequency function in a swept sine measurement. Because of the peak reduction when passing the impulse through the All-Pass filters, however, it is beneficial to have an invertible filter which can maximize the dynamic range of the signal over time by normalizing the amplitude envelope. The inverse of this filter can then be applied before feeding the signal back through the all-pass network.

3.8.3 Transient Noise

Transient sounds that occur during measurement can also pollute the estimated responses. Because of the phase randomization of noise type measurements, transient noises will be scattered across the whole measurement time, whereas because of the deconvolving process when using swept sines, transients will be manifest as sine sweeps in the opposite direction.

Since wind instrument measurements take place in a controlled environment where external transients can be minimized this transient noise immunity is less of a concern than in totally uncontrollable environments, such as room acoustics measurements where a truck may pass by, other people may be in the building, or sound may leak in through windows.

3.8.4 Non-linearity

The usable signal-to-noise ratio of MLSs compared to other methods is closely related to the level at which the signal can be driven and how non-linearities manifest themselves. The effect of non-linearity in MLSs have been studied extensively in Vanderkooy (1994), which shows any non-linearity present in the measurement is distributed over the whole measurement period, therefore minimizing the concentration of non-linearities as the period L of the MLS increases.

The rejection of non-linearities from swept sine measurements means that they can be driven at a louder volume than MLSs, since non-linearities within the driver and tube will be pushed out from the linear response. When compared to the swept sine's total rejection of non-linear effects, the MLS is much less predictable and fares more poorly.

When using a logarithmically swept sine it is possible to not only separate the non-linear response from the linear, but, if the sweep is slow enough, measure each level of harmonic distortion. Farina (2000) gives a comparison of non-linearity measures using swept sines in contrast to traditional measures of non-linearity using single sine tones. The method produced results of comparable quality more quickly and easily.

3.8.5 Overall Comparisons

Most reviews of stimulus signals have concentrated on MLSs and sine sweeps because the other stimulus signals presented have limited applicability. All-pass sequences seem a good choice if many measurements using small stimulus signals are desired. Golay codes seem a good choice if it is necessary to have a binary test sequence which is of length 2^N instead of $2^N - 1$. The OATSP is less flexible to design than the swept sine method and is similar in most regards.

One of the reasons for MLSs historical popularity has been the simplicity in generating the stimulus signal, without requiring an FFT. This, however, is no longer a concern for most measurement scenarios, especially those for wind instrument reflectance measurements. The benefits over chirp stimulus given in Rife (1989) were based on swept sine methods using deconvolution methods which have been displaced by those with better signal-to-noise ratios and harmonic distortion immunity.

MLS measurements reject most of the DC component of a measurement system, a benefit if the final reflectance measure is going to be used to reconstruct the bore profile, where a DC offset will cause a diameter drift in the calculated profile.

Time aliasing problems that can be present with periodic testing can be avoided with sine sweep techniques. Even if there is no silence after the sweep, care can be taken with deconvolution so that even if the response measured is truncated, there won't be any wrap around of the end of the impulse response onto the beginning.

Farina (2000) also describes how swept sine techniques seem better at exploiting the bit depth of modern DACs. Little improvement was shown in MLS measurements by increasing the bit depth from 12 to 16 or 20 bit, but the increase from 16 to 20 bits with swept sines yielded cleaner results. Significant improvements were not found when raising the depth from 20 to 24 bits.

Chapter 4

Pulse Reflectometry Improvements

4.1 Longer Stimulus Signals

Existing pulse reflectometry systems usually use short duration stimulus signals, such as band-limited chirps or bursts of noise, to drive the system. These are designed to have a practical length of less than T_{M-O} , the time it takes for sound to propagate from the object back to the microphone. With this constraint the reflection function can be easily found from the raw pressure signal by windowing the object reflections and deconvolving the pulse shape $f(t)$ measured in the calibration step from them.

It is possible to greatly increase the signal-to-noise ratio of the measured reflection function by using stimulus signals longer than T_{M-O} , which can then be deconvolved from the pressure signal to recreate the system impulse response. This section discusses the procedural changes needed when using much longer stimulus signals in a pulse reflectometry system.

4.1.1 Theory

Recall the description of the microphone signal in a pulse reflectometry setup given in Chapter 2:

$$\begin{aligned}
 s(t) = & f(t) + f(t) * r_o(t) * \delta(t - T_{M-O}) + \\
 & f(t) * r_o(t) * r_s(t) * \delta(t - (T_{M-O} + T_{S-M})) + \\
 & f(t) * r_o(t) * r_s(t) * r_o(t) * \delta(t - (2T_{M-O} + T_{S-M})) + \dots \quad (2.7)
 \end{aligned}$$

If we probe the system with a stimulus signal $x(t)$ instead of an impulse the equation

for the microphone signal will be:

$$\begin{aligned} s'(t) = & x(t) * f(t) + x(t) * f(t) * r_o(t) * \delta(t - T_{M-O}) \\ & + x(t) * f(t) * r_o(t) * r_s(t) * \delta(t - (T_{M-O} + T_{S-M})) \\ & + x(t) * f(t) * r_o(t) * r_s(t) * r_o(t) * \delta(t - (2T_{M-O} + T_{S-M})) + \dots \end{aligned}$$

assuming that all of the interactions within the tube are linear and time-invariant. Note there is no requirement that the length of $x(t)$ be less than T_{M-O} .

Since we have $x(t)$ stored, we can deconvolve the stimulus signal from the measured pressure signal $s'(t)$ as discussed at the beginning of Chapter 3. Because deconvolution is commutative, the result of deconvolving $x(t)$ from $s'(t)$ is exactly $s(t)$. After deconvolution we can treat the measured signal as before and the reflection function can be windowed out of the signal, again assuming that $f(t)$ is shorter than T_{M-O} and that the reflection function $r_o(t)$ is shorter than T_{S-M} .

This depends on linearity in the source tube and linear interaction with the object being measured. Non-linearities in the measurement will be manifest as errors in this primary deconvolution, since deconvolution of $x(t)$ from $s'(t)$ will not completely reconstruct $s(t)$. Methods that reject non-linear distortion and have superior signal-to-noise ratios will more accurately reconstruct $s(t)$ from $s'(t)$.

As discussed in Chapter 3, this deconvolution can be performed in the frequency-domain by simply dividing the pressure measurement by the stimulus signal, provided there is energy across the frequency range. After deconvolution of the stimulus signal from the raw response we can treat the measured signal as before and impedances can be calculated from the measured reflection function.

4.1.2 Verification

To verify the theory, a calibration measurement of a pulse reflectometry system was performed with a repeated pulse train and again with a swept sine stimuli. All pulse reflectometry measurements presented in this thesis were made using a system designed and constructed by Antoine Lefebvre. The apparatus consists of a 5 meter long aluminum pipe, with a microphone placed halfway down the length of the pipe.

For repeated pulse testing, where $f(t)$ is shorter than the object to microphone travel time T_{M-O} an impulse was repeated 64 times with a period of 0.69 seconds over a 44.3 second period. Figure 4.1 shows part of a calibration measurement taken of a pulse reflectometry setup using repeated pulse testing.

The calibration measurement was repeated, this time using a single 43.6 second logarithmically swept sine going from 20 Hz to 18000 Hz to stimulate the system. The unprocessed pressure measurement from the microphone, $s'(t)$ is shown in Fig. 4.2.

The swept sine makes better use of the dynamic range of the system than repeated pulse testing, driving the system with much more signal energy. The range is attenuated

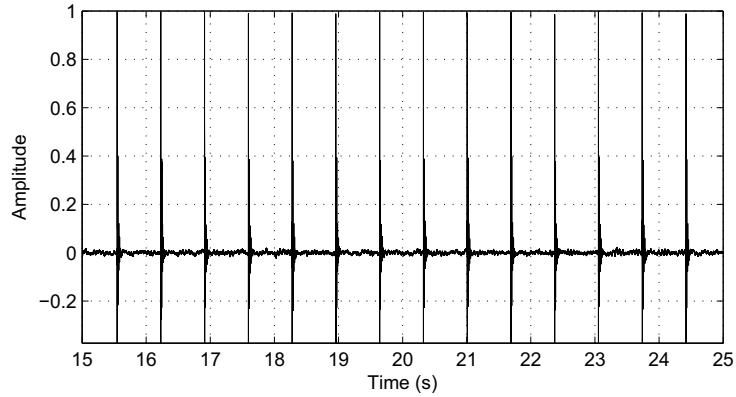


Figure 4.1 The pressure signal from a pulse reflectometry calibration measurement when using repeated pulse testing.

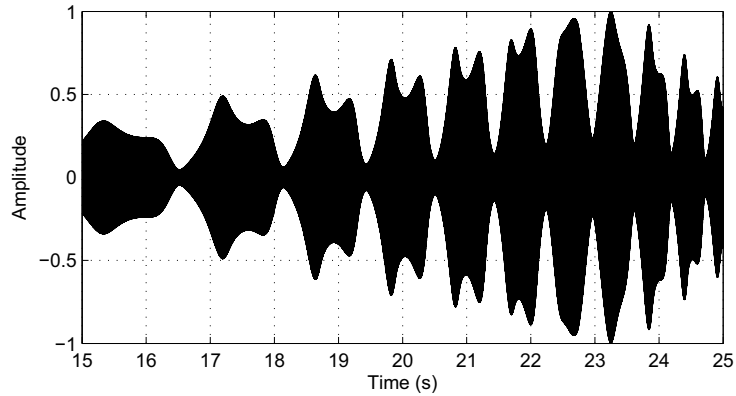


Figure 4.2 The pressure signal from a pulse reflectometry calibration measurement when using a swept sine stimulus.

at the beginning and end because of poor response of both the driver and microphone at high and low frequencies.

The raw response was then windowed to be the same size as the stimulus signal to simplify deconvolution. While the end of the raw response is prematurely cut off, the result is a small loss of the high frequency response well above the cut-on frequency for higher order modes. It is also possible to zero pad the stimulus signal so the end of the high frequency response isn't truncated.

Plots of the system impulse responses measured from repeated pulse testing and swept sine measurements, after averaging and deconvolution respectively, are shown in Fig. 4.3. The repeated pulse plot is the result of averaging the 64 measured responses, while the

sine sweep is the result of deconvolving the stimulus from the measurement with frequency domain deconvolution.

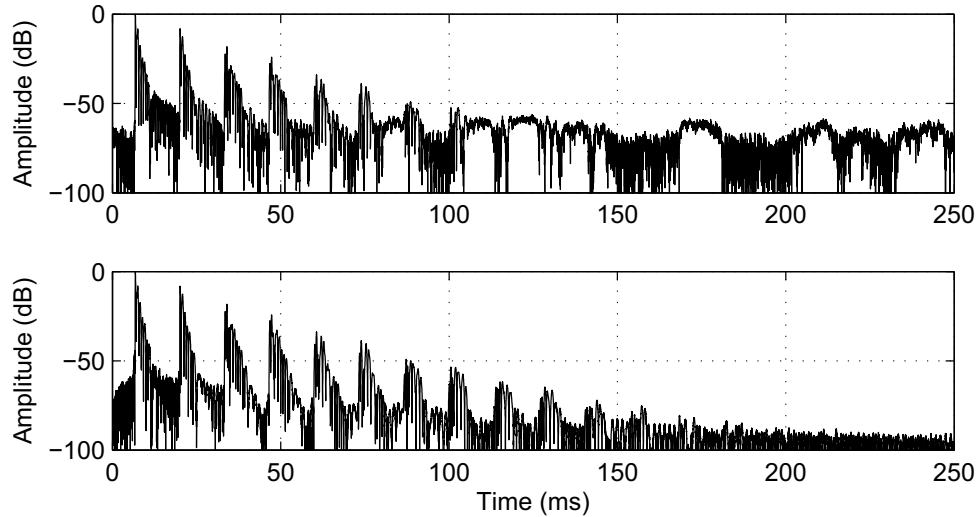


Figure 4.3 The impulse response of a calibration measurement of a pulse reflectometry system stimulated using repeated pulse testing (top) and swept sine testing (bottom) on a log scale.

Figure 4.3 illustrates a significant improvement in signal-to-noise ratio when using the longer duration stimulus, with a noise floor on the order of -90 dB instead of about -60 dB. Because doubling the number of averages will only reduce the uncorrelated noise by 3dB, even with a 64 repetitions of the pulses, the noise floor remained around -60dB. The swept sine measurement achieved an extremely good signal-to-noise ratio primarily because the stimulating signal put much more energy into the system, lowering the noise floor and increasing the dynamic range of the measurements.

The plots show the pulse $f(t)$ as it passes by the microphone, hits off the rigid termination and ricochets inside the source tube, reflecting off the driver and end cap. The first few pulses passing the microphone are plotted on a linear scale for repeated pulse testing and a swept sine stimulus in Fig. 4.4.

The shape of the pulses is nearly identical in the two methods, with the exception of some high frequency ringing before each pulse. This is likely because the swept sine signal lacked energy at high frequencies, resulting in a small amount of noise after the deconvolution process.

Because of viscothermal losses, the finite impedance of the driver and the coupling between it and the source tube, $f(t)$ is a distorted impulse, smeared over a short time. After a delay of T_{M-O} the attenuated pulse appears again after reflecting off the rigid cap. Because the pressure reflection coefficient of the rigid end is +1, the reflected pulse is

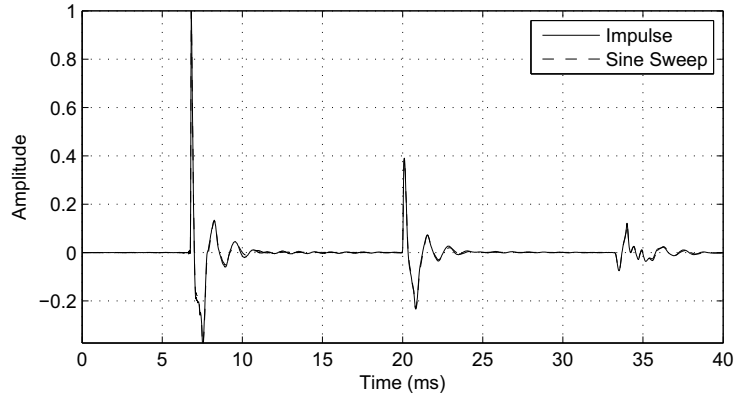


Figure 4.4 The impulse response of a calibration measurement of a pulse reflectometry system stimulated using repeated pulse and swept sine testing on a linear scale.

generally of the same shape with no inversion.

After a further delay of T_{S-M} the pulse appears again, this time more heavily distorted because of its interaction with the driver and coupler between the driver and source tube. The third pulse, which corresponds to $f(t) * r_o(t) * r_s(t)$, is basically the same in both the repeated pulse test, where the driver is likely nearly stationary, as it is in the swept sine method, where it is being driven. This implies that the source reflection is predominantly linear and means there is a good chance that we can deconvolve out source effects, as is discussed in Section 4.2.

As before we can window the measured reflection function $r_o(t)$ if it has a practical length of less than the round trip microphone to source travel time T_{M-S} , and deconvolve out driver, source tube and sensor effects.

This novel improvement to pulse reflectometry measurement means the signals presented in Chapter 3 can now be used to measure reflection functions. The fitness of each signal type in the face of degrading factors is not exactly the same for reflection function measurements as for impulse response measurements. The signals from Chapter 3 are therefore compared with regard to pulse reflectometry impedance measurements in the next section.

4.1.3 Comparison of Stimulus Signals

A computational model of a pulse reflectometry system was created using a digital waveguide simulation of a cylindrical bore to test the effectiveness of each of the signals described in Chapter 3 when measuring reflection functions. The model simulates a complex input signal traveling within a cylindrical waveguide that is terminated with either a radiation filter approximating an open end or a infinite impedance filter reflector approximating a

closed end. The driver is modeled as an infinite impedance reflector.

The waveguide uses lumped filters at the source, microphone and open end to incorporate viscothermal losses based on Keefe (1984) and, when the end is open, a fourth-order filter approximation (Scavone, 1997) of the radiation characteristics of an unflanged pipe as reported by Levine and Schwinger (1948). The purpose of the simulation is to see how degradational effects will be manifest in measurements of the reflectance and calculations of the impedance of the open-end filter. The reflectance of the filter is shown in Fig. 4.5. Note that the filter design parameters were made to match the theoretical values well at lower frequencies at the expense of some irregularities that appear in the upper frequency range.

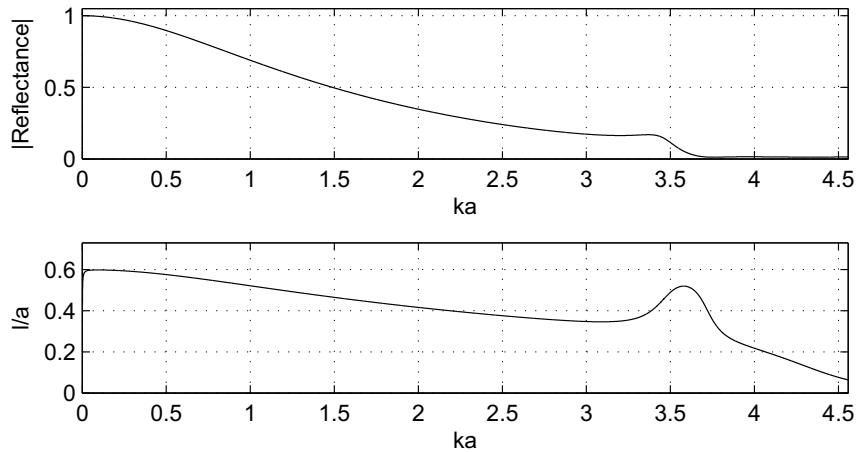


Figure 4.5 The reflectance of the open-end filter approximating the results of Levine and Schwinger (1948).

The experimental procedure was the same as for physical pulse reflectometry measurements. The reflection function from the open-end filter was measured when the waveguide was stimulated with the signal types described in Chapter 3 and then converted to a frequency domain reflectance. The reflectance from the rigid termination was deconvolved using division in the frequency domain and impedance was then calculated from the reflectance using Eq. 2.4. The results from the contaminated measurements are plotted along with the calculated input impedance of the open-end filter, as shown in Fig. 4.6.

Impulse testing averaged four sequential impulse measurements, with the period set so that minimal time aliasing of the response occurred. MLS and noise sequences were half the length of the swept sines and were repeated twice because of their deconvolution requirements. Golay codes were each played for an eighth the time of the other signals to allow the system to return to its initial state, lowering the amount of energy in the system. The swept sines and OATSPs were played only once through the system.

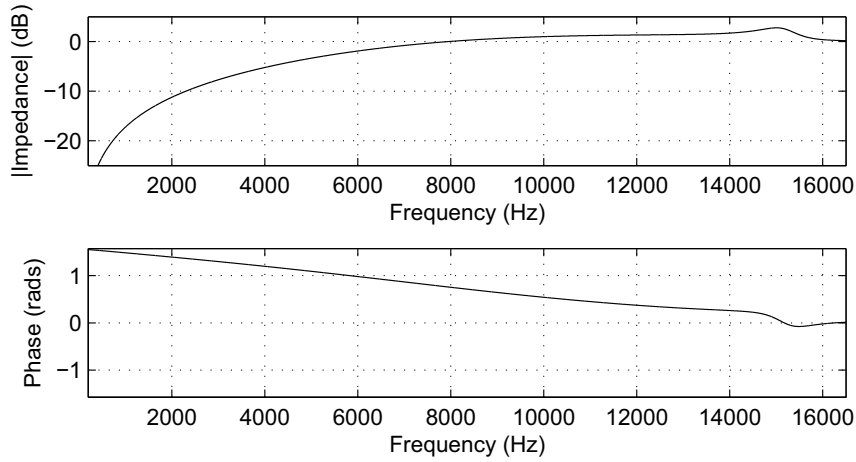


Figure 4.6 The impedance of the open end filter calculated using the reflection function of Fig. 4.5.

When simulating non-linearities, the input signals were first normalized so the peak value was at a certain dB value relative to 0 dB. The signals were then passed through a simple cubic soft-clipper, limiting the peak value to 0 dB, before being fed to the waveguide model. Resistance to white-noise pollution was tested by normalizing each of the signals, feeding them to the waveguide and adding uncorrelated noise to the waveguide response at -60dB, -40dB and -10dB before deconvolution. How DC offsets affect measurements was tested by adding a DC offset to the signal before it was fed to the waveguide.

The results obtained using various stimulus signals in the presence of a weak non-linearity, uncorrelated white noise, and a DC offset are discussed in the following subsections.

Non-linearities

Waveguide simulations do not experience distortion of the signal at the driver, microphone or by transmission within the bore when overdriving the signal, which means that the gain of each signal can easily be maximized and compared between measurement types. In actual measurement scenarios this maximizing of the signal-to-noise ratio can be quite difficult.

Since the deconvolution of signals and the pulse shape from the results depend on the linearity of interactions within the source tube, it is important to avoid driving the system in a non-linear fashion. Detecting the presence of non-linearities in actual measurements can also be difficult and depends on the stimulus signal used. Swept sine signal types make it easier to see if the system is being driven in a non-linear fashion, as higher harmonics begin to appear in the spectrogram of the microphone response. Noise-based signals like MLSs

and Golay codes, which excite many frequencies simultaneously, have no easy measure to avoid distortion.

To simulate the effect of non-linearities on calculated impedances, each stimulus signal was passed through a simple cubic non-linear system, reducing the peak value by a specific dB amount, before being fed into the waveguide simulation. The signals generally behaved similarly depending on whether they were noise or swept sine based.

Because the non-linear modelling was very simple, all of the two-value signals, Golay Codes, MLSs and impulses, showed no change whatsoever in calculated impedances. Since a standard cubic soft-clipper is deterministic and memory-less the shape of each of these signals was not modified at all, even though their range might be.

It's reasonable to assume that in actual measurement scenarios, non-linearities would affect MLSs and Golay codes similarly to how they affected the random noise signal type, shown in Fig. 4.7. This is because even though they are theoretically two-value signals, they will be realized as more complex signals at the loudspeaker, where non-linear distortion is likely to occur.

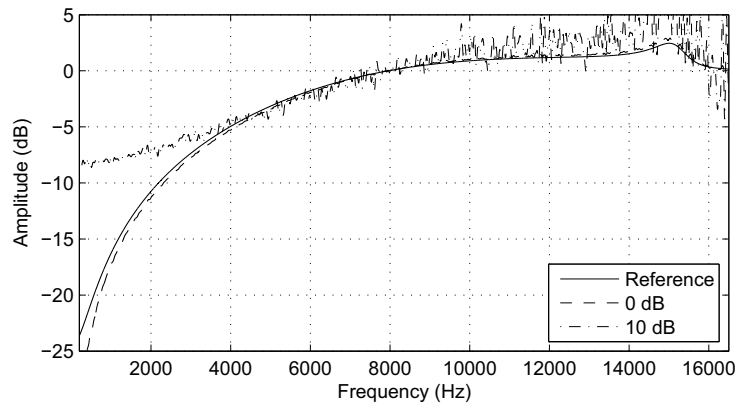


Figure 4.7 Calculated impedance of the open end of a circular cylindrical pipe using noise in the presence of non-linear contamination.

These signal types are the most susceptible to distortion from non-linearities because of their low peak-to-signal ratio. The signal is usually at a level high enough to be effected by non-linearity and as such even in the presence of moderate non-linear distortion the calculated impedances are heavily changed. Golay codes will show slightly more resistance to non-linear distortion because of inserted silence necessary between the codes.

Logarithmic sine sweeps reject non-linear artifacts very well, as can be seen in Fig. 4.8. When the peak value is reduced by 10 dB the shape of the impedance curve is still predominantly maintained. Even when the peak value is reduced 40 dB it is still possible to make out the original curve shape, although there is a large peak at 12 kHz not present

in the original. Linear sine sweeps are similar, although the impedance curve is a little smoother at high frequencies.

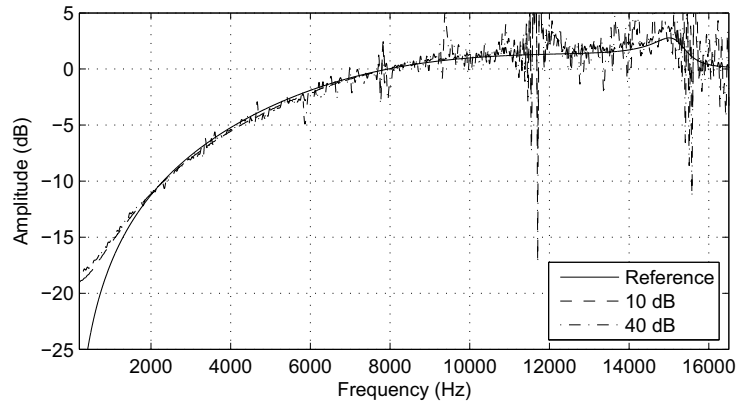


Figure 4.8 Calculated impedance of the open end of a circular cylindrical pipe using a linearly swept sine in the presence of non-linear contamination.

Figure 4.9 shows that the OATSP also fared well in the face of non-linearities, suffering from distortion at low and high frequencies, but in a smoother way than the linear or logarithmically swept sine. Like MLSs and sine sweeps, the OATSP uses the full dynamic range of the system, however much of the generated OATSP is a low-level signal to avoid discontinuities, increasing the peak-to-signal ratio.

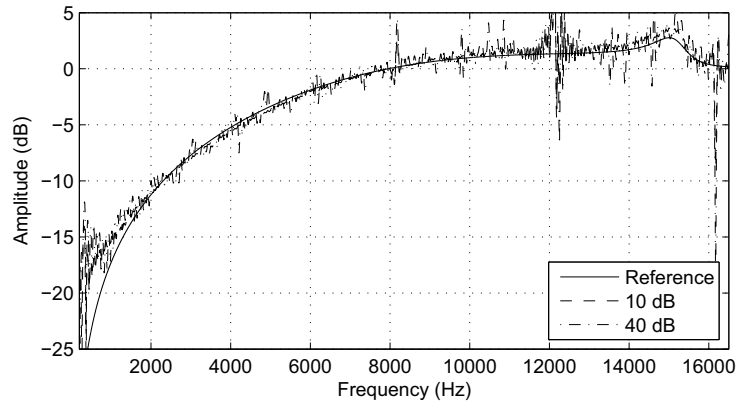


Figure 4.9 Calculated impedance of the open end of a circular cylindrical pipe using an OATSP in the presence of non-linear contamination.

In the simulations impulse testing most accurately recreated the reference impedance in

the face of strong non-linearities, however in real measurements the susceptibility to white noise pollution makes them a poor choice in most situations.

While it is important that a stimulus signal yield good results in the presence of mild non-linear effects, another key consideration should be how easy it is to detect when non-linearities occur. Because non-linearities are most often present when the speaker is driven too hard, non-linearity can generally be avoided by setting the output to a reasonable level.

Swept sines and OATSPs allow one to easily to detect the presence of non-linearities because they have a smoothly varying instantaneous frequency. When using these signals, non-linearities appear in the raw response, before deconvolution, as energy at different frequencies. When using noise measurements it is more time-consuming to determine whether non-linear effects are present and thus setting the level to maximize the signal-to-noise ratio of the measurements is more difficult.

White Noise

Uncorrelated white noise was added to the microphone signal to see how well each method responded to adverse measurement conditions or substandard apparatus. A white noise signal of the same length at the response was created and mixed into the output signal at each of the levels.

Impulse measurements are extremely susceptible to distortion from noise pollution even at very low levels, as shown in Fig. 4.10. A greater numbers of averages increases this resistance, however measurement time must be dramatically increased.

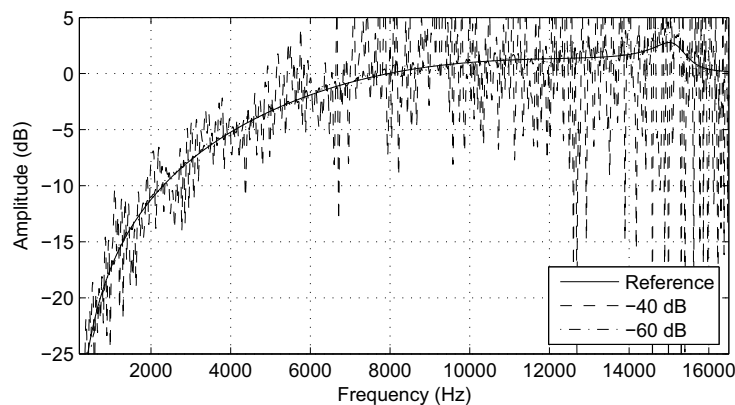


Figure 4.10 Calculated impedance of the open end of a circular cylindrical pipe using a repeated pulse testing in the presence of uncorrelated white noise.

Golay Codes, MLSs and Noise all showed a more erratic result, increasing in intensity with frequency in the presence of added uncorrelated white noise. Figure 4.11 shows

impedances calculated from measurements with MLSs which, with their low peak-to-signal ratio, recreated the impedance curve more accurately than the other two methods.

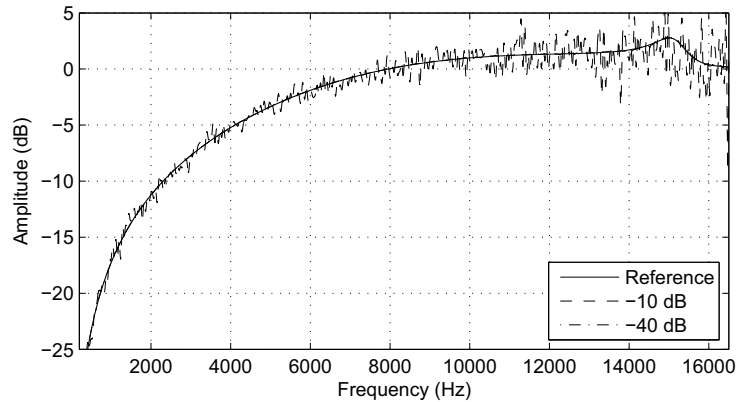


Figure 4.11 Calculated impedance of the open end of a circular cylindrical pipe using an MLS in the presence of uncorrelated white noise.

Uncorrelated white noise affects impedances calculated using the OATSP and both sine sweeps similarly. All three recreated the theoretical impedance almost up to the Nyquist frequency, even in the presence of a -40dB noise floor. Even with -10 dB noise the overall shape is well preserved at low frequencies, with the linear sine sweep reconstructing the impedance slightly more accurately.

Swept sines do offer the maximum signal-to-noise ratio for certain measurement time because of the large amount of signal energy and the fact that they do not need to be repeated. If the spectrum of the contaminating noise is known, it is also possible to custom design a path for the sweep that will concentrate energy at frequencies which will be most effected by background noise. Noise-type signals can also have certain frequency energy pre-emphasized, however the procedure is slightly more complicated, as a pre-emphasis filter and its inverse must be constructed.

DC offset

Layer peeling algorithms require that there is no DC offset present in the measured reflection functions, meaning stimulus signals that reject a DC offset are preferable if a bore profile reconstruction is to be made from the pulse reflectometry measurement. Currently DC offsets must be removed manually to avoid drift in the radius over axial distance. To test the effect of this, a constant value was added to the whole signal before it was fed into the waveguide, adding a positive DC offset to the signal.

The input impedance calculated from impulse testing in Fig. 4.12 show that DC offsets create an oscillation in the impedance over the whole frequency range. Even small DC

offsets result in large variations in impedance.

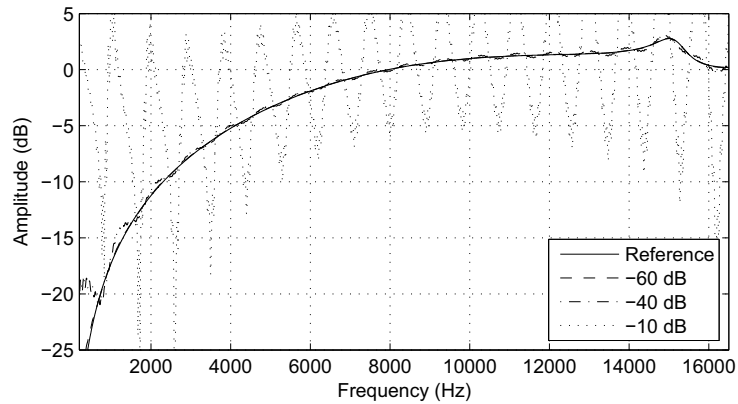


Figure 4.12 Calculated impedance of the open end of a circular cylindrical pipe using a repeated pulse testing in the presence of a DC offset.

Golay Codes, MLSs and noise signals all completely eliminate any DC component in the system with absolutely no distortion in the impedance.

Linear swept sines do a good job of limiting the effects of moderate DC offsets, however as shown in Fig. 4.13 there is slight distortion in the case of very extreme added offsets.

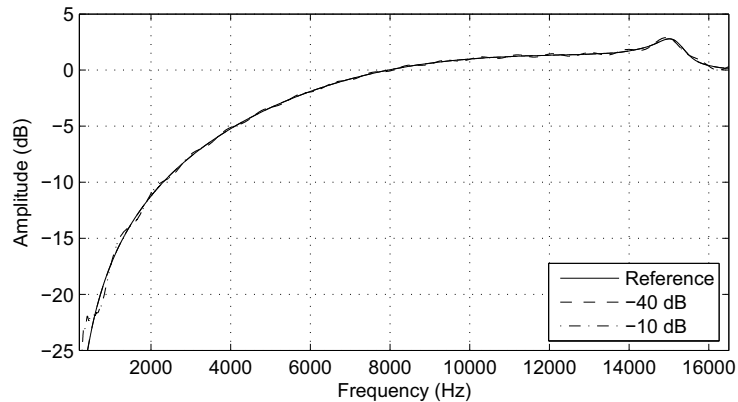


Figure 4.13 Calculated impedance of the open end of a circular cylindrical pipe using an OATSP in the presence of a DC offset.

Logarithmic swept sines and OATSPs are preferable to linear sweeps, rejecting the effects of even extreme DC offsets entirely.

MLSs and Golay codes, with their ability to completely eliminate any DC component in the system, have an advantage in this regard, however there are a number of methods

for removing DC offsets from the deconvolved results. If those methods can safely be used instead, the benefits of the swept sine methods to reject non-linear components and their decent handling of DC offsets make them preferable for taking the measurements.

4.2 Pulse Reflectometry Window Size Effects

The reflection function of an acoustic body corresponds to the system response to a pressure impulse at the input, assuming the input is terminated anechoically. Anechoic termination can be approximated by affixing a sufficiently long tube to the input so that waves traveling toward the input are not disrupted, as they would be from a discontinuity, and are reflected back into the body only after a sufficient measurement time. This means that reflection function measurements from pulse reflectometry are only valid before reflections off the source return and reenter the instrument.

The measured reflection function must be shorter than T_{S-M} , the round trip travel time between the source and microphone, as afterwards the reflection function convolved with the source reflectance will pass by the microphone again. Diameter discontinuities between the source tube and the object to be measured also complicate reflection function measurements, since any pressure component leaving the entrance to the object will be partially reflected back in. This stimulates the object again and violates the non-reflecting source constraint.

To estimate the effects and the limitations on impedance measurement of the discontinuity and windowing of the source reflection, the model used in the last section was modified so that source reflections were optional and so that a cylindrical test object of a different diameter could be attached to the end. Models of the cylindrical test objects were also made using frequency-domain transmission matrix techniques that more accurately represent the open-end radiation and transmission characteristics.

Measurements of the input impedance of two cylindrical bores, with 6mm radii and lengths of 55.9cm and 84.9cm, were calculated from reflection functions simulated in the waveguide models and compared against the matrix model to see the effects of diameter discontinuities, the reflecting source and the size of the window. Actual cylinders of these lengths were then measured using a physical pulse reflectometry system and compared against the modelled data.

The measurement apparatus was constructed to simulate the physical measurement apparatus. The 5 meter-long source tube has the microphone positioned halfway along the bore, making $T_{S-M} = T_{M-O} = 14.5$ ms, or 696 samples at a sampling rate of 48 kHz. The first measurements were made with a window size of 696 samples so that only reflections from the instrument were included in the reflection function.

If the reflecting characteristic of the driver is, or can be approximated by, +1, corresponding to an infinite impedance reflector, then it should be possible to include the reflections off of it in both the calibration and object measurements, increasing the length

of reflection functions that can be measured to $T_{S-M} + T_{M-O}$ or 1392 samples.

This means both measures then include the first reflection off the source, but no subsequent reflections from the object. The sections labeled "Source Reflections" test whether this approximation is reasonable by comparing of impedances calculated from reflection function measurements with the larger windows to previous measurements and theoretically predicted values.

4.2.1 Short Cylinder

Modelled Results

The waveguide simulation was first set up to take measurements without the effects of source reflections, allowing the reflectance to die away over 100 dB over the course of the measurement window, and without modelling the discontinuity at the junction between the source tube and modelled cylinder. A calibration measurement of the model was taken and deconvolved from the measurement of the cylinder. The impedance calculated from the waveguide using a sine sweep is plotted against the theoretical impedance calculated from the matrix model in Fig. 4.14.

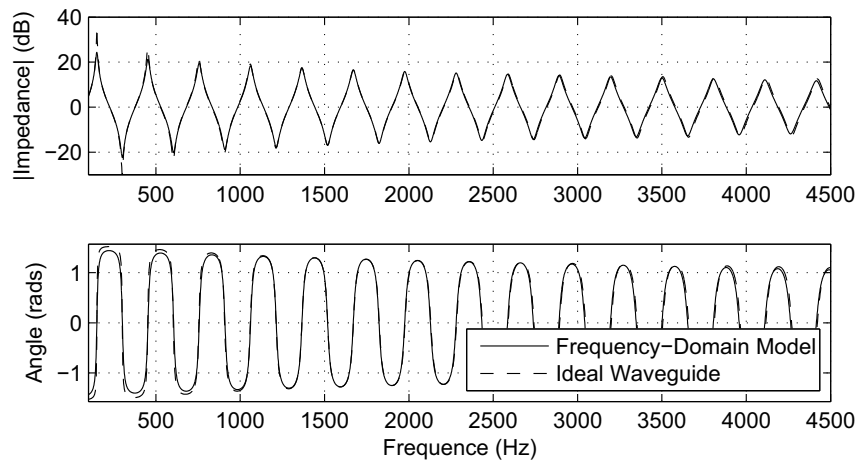


Figure 4.14 The input impedance of a short cylinder predicted using a frequency-domain method plotted against the input impedance calculated from a waveguide model.

The impedances calculated from waveguide simulations using impulses, sine sweeps and MLS testing showed almost no difference across the whole frequency range. The slight variation at low and mid frequencies between the waveguide and frequency-domain predictions is due to the digital filter approximations for viscothermal losses and the open-end radiation matching theoretical results poorly at extreme high and low frequencies.

This model does not account for the scattering which will occur at the junction between the probe tube and the acoustical system because of the diameter discontinuity. Because no reflections occur here, the theoretical length of the reflection function is the round trip travel time plus the length of the filter approximating the open end. This is the same with a reflecting source, regardless of the type of stimulus signal used. A waveguide modelling the source as an infinite impedance reflector showed nearly identical results over the whole frequency range, regardless of the stimulus signal used.

A diameter discontinuity will result in a change of the characteristic impedance at the junction between the two bores because of their differing diameters. This change results in partial transmission and reflection of pressure traveling past this point. A Kelly-Lochbaum (Kelly and Lochbaum, 1962) scattering junction assumes the continuity of pressure and conservation of volume flow across the boundary and incorporates the differences in characteristic impedance to calculate how traveling pressure is effected.

When this junction is added to the waveguide model, the impedance calculated from the reflection function changes dramatically. Figure 4.15 shows impedances calculated from the waveguide with a scattering junction using various stimulus signals. This waveguide simulated an anechoic source termination, so the reflection function could be measured until it drops off more than 100 dB. The addition of the junction increases the length of the reflection function dramatically, since energy leaving the body is partly reflected back in, stimulating the object again.

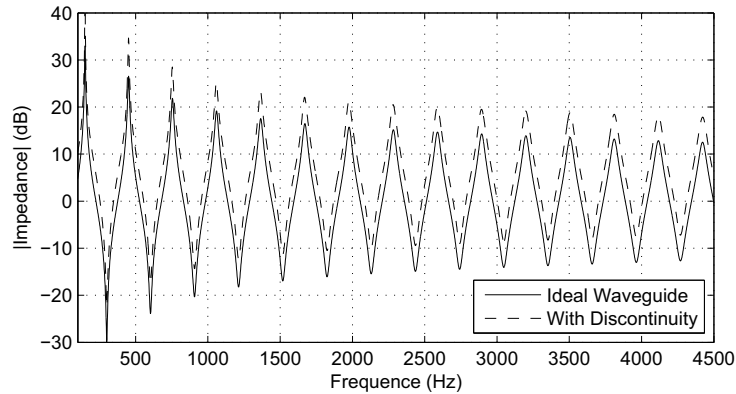


Figure 4.15 The input impedance of a short cylinder calculated from a waveguide model of a pulse reflectometry system that models a diameter discontinuity between the source tube and the cylinder.

The calculated impedance is offset from the theoretical prediction by 5.53 dB across almost the entire frequency range. This corresponds to a ratio of 1.8906 times the reference impedance, which is equal to the ratio of the cross sectional area of the source tube to the cross sectional area of the cylinder. Incorporating a -5.53 dB offset to the results calculated

from the waveguide with a scattering junction result in a near perfect match to the predicted impedance.

The waveguide was further modified to incorporate a reflecting source, modelled as an infinite impedance reflector. Because the discontinuity was included in the model, the offset in the calculated impedance was present, but is corrected for in Fig. 4.16. With a reflecting source the reflection function could only be used for 696 samples to avoid including reflections from the source.

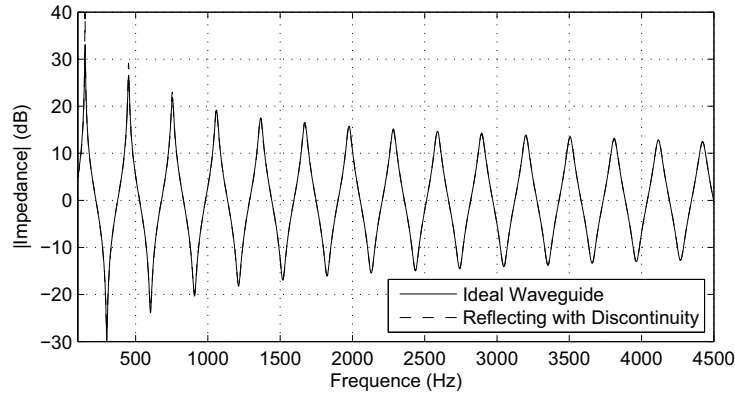


Figure 4.16 The input impedance of a short cylinder calculated from a waveguide model of a pulse reflectometry system that models a diameter discontinuity between the source tube and the cylinder and a reflecting source.

Input impedance calculated for the small cylinder was almost unaffected by windowing the reflection, agreeing to within 0.3 dB of the non-reflecting source model, except at the resonances and anti-resonances in the low frequency range. A plot of the difference between the impedance from an ideal waveguide, with a non-reflecting source and no scattering junction, and one from a more robust model of the physical pulse reflectometry system is shown in Fig. 4.17.

This difference is due to the truncation needed to simulate a non-reflecting source, which is even more pronounced because the scattering junction greatly increases the length of the reflection function. If the source is simulated as an anechoic termination or if the source tube length is sufficiently increased, the impedance calculated from the model is exactly that of the attached system plus the offset induced by the diameter mismatch.

The locations of maximum difference in Fig. 4.17 correspond to the resonances and anti-resonances of the cylinder, with the increased impedance at the anti-resonances being the largest. Here we can see that the difference is mainly concentrated in the low-frequency range below 2000 Hz.

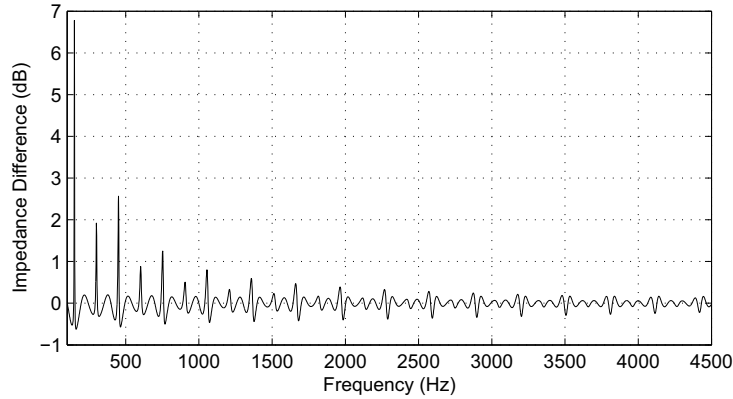


Figure 4.17 The difference between the input impedance calculated from a pulse reflectometry model incorporating a diameter discontinuity and reflecting source and an ideal pulse reflectometry system

Measured Results

Real pulse reflectometry measurements were taken of matching bores to compare with the theoretically predicted impedances. Measurements were done with a sampling rate of 48kHz using a Sennheiser KE4 microphone capsule plugged into a Unides Microphone Preamp with the gain set at the minimum (26dB). This was attached to the first line input of the RME Fireface 800, with the software gain set to +4 dBu.

All measurements were performed at within 0.1 degrees of 22.2 degrees Celsius. The maximum amplitude of the swept sine stimulus used was 0.5, with software gains for the internal audition mix set at -3.1 dB, and the audition to headphone out gain set to -3.1 dB to avoid distortion at the DAC. These settings were kept constant for all measurements, using both the swept sine and MLS stimuli.

Calibration measurements were taken to measure the pulse shape and propagation losses with the source tube rigidly terminated. The rigid cap was then removed and the cylinders were attached and measured using the same stimulus signals.

For these measurements both the calibration and cylinder measurements were windowed to be of length T_{S-M} . The impedance calculated from the short cylinder measurement is plotted with the impedance predicted using the frequency-domain approach in Fig. 4.18. The impedance calculated from the measurement is plotted with an empirically determined offset of -3.7 dB to correct for the diameter discontinuity between the source tube and cylinder in Fig. 4.18. This differs from the 5.53 dB offset which is expected given the ratio of the source tube and cylinder radii.

The speed of sound for the matrix simulation was set to be 346.25 meters per second so that the resonance and anti-resonances were closely aligned with the other impedance curve. The predicted speed of sound given the real measurement conditions is $331.3 + 0.6 * 22.2 =$

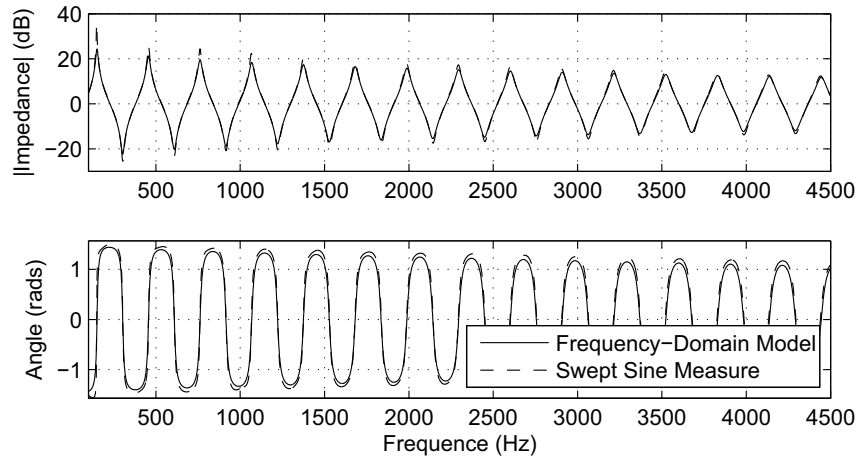


Figure 4.18 The input impedance of the short cylinder predicted from a frequency-domain model and calculated from measurements taken from a pulse reflectometry apparatus.

344.62, somewhat lower than the empirical match. It is possible the discrepancy is due to air density and altitude variation, but the most likely explanation is that the viscothermal losses incorporated in the model do not completely characterize the real losses.

The difference between the magnitudes of the input impedances is plotted in Fig. 4.19, showing the impedance calculated from the measurement closely matches the theoretically predicted one below the duct's cut-on frequency. Because the diameter discontinuity greatly increases the length of the reflection function, it must be windowed, resulting in the differences at low frequencies.

The difference from the measurement shown in Fig. 4.19 and the predicted difference show in Fig. 4.17 are somewhat similar. Variation is still the greatest at the resonances and anti-resonances, especially at low frequencies. The most notable difference is that, when the discontinuity offset is taken into account, the calculated anti-resonances are below those predicted by the model. When the model incorporated a reflecting source and a scattering junction simulation the anti-resonances were shifted upward from the predicted values whereas in the measurement these values were lowered.

There are also more extreme differences at low frequencies in the resonances and anti-resonances from the measurement than those predicted by the model. As the frequency increases above 3.5 kHz the locations of the resonances and anti-resonances stray from their predicted positions.

These differences may be because the model is one-dimensional and system it is modelling is three-dimensional. However, the most likely cause is a discrepancy between the loss predictions incorporated using digital approximations and the losses which actually occur.

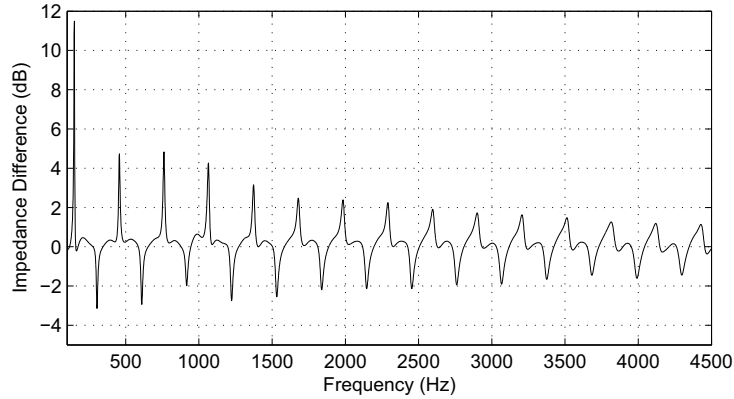


Figure 4.19 The magnitude difference between short cylinder input impedances calculated using a frequency domain model and those calculated from a pulse reflectometry apparatus

These findings are consistent with the modelled results shown earlier, indicating that in the presence of reflection function truncation the greatest difference between the measured results and the theoretically predicted results is found at low frequencies. The measured results are generally accurate for an object that is much smaller than the source tube, however, and there is good agreement between the theory and measurements.

Source Reflections

The impedance was also calculated using calibration and measurement windows of length $T_{M-O} + T_{S-M}$ instead of just T_{S-M} to include the first reflection from the source. The impedance calculated using the larger window is plotted against the theoretically predicted input impedance in Fig. 4.20 and a plot of the difference is shown in Fig. 4.21.

The most significant effects of incorporating a source reflection occur below 2 kHz, where the resonances are closer to their theoretically predicted values and the anti-resonances are slightly further away. The regions between the resonances and anti-resonances also show more variation, especially around 1000 Hz, where transitions between the extremes are more jagged, which may be because the source is likely not a perfect reflector approximated by a reflection coefficient of +1, as is assumed. The resonances and anti-resonances above 4000 Hz are also very slightly shifted from their previous locations, putting them even further from their theoretically predicted positions.

The differences here are at a level below those in Fig. 4.19, meaning that incorporating source reflections does result in more accurate values for the low-frequency resonance.

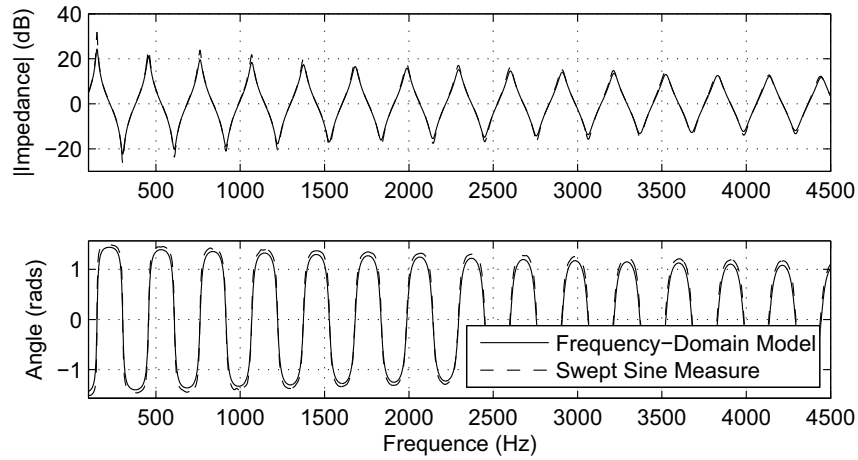


Figure 4.20 The input impedance of the short cylinder predicted from a frequency-domain model and calculated from measurements that incorporate source reflections taken from a pulse reflectometry apparatus.

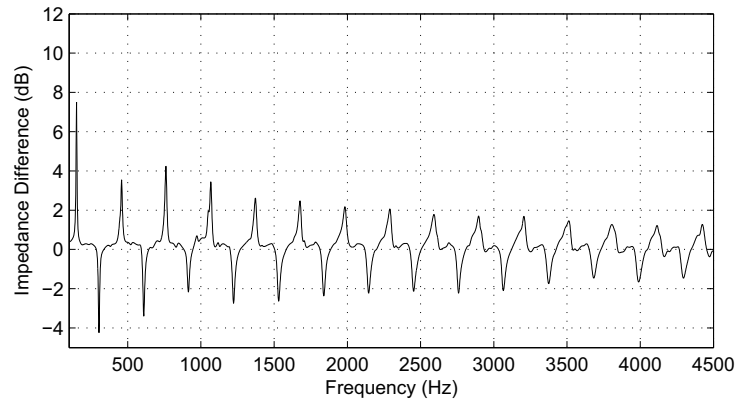


Figure 4.21 The magnitude difference between short cylinder input impedances calculated using a frequency domain model and those calculated from a pulse reflectometry apparatus, including source reflections.

4.2.2 Longer Cylinder

Modelled Results

The simulations from Section 4.2.1 were repeated with the dimensions of the longer cylinder. The impedance calculated from an ideal waveguide simulation, which has an anechoic source and no discontinuity between the source tube and cylinder, is plotted against an impedance predicted using a frequency domain model in Fig. 4.22.

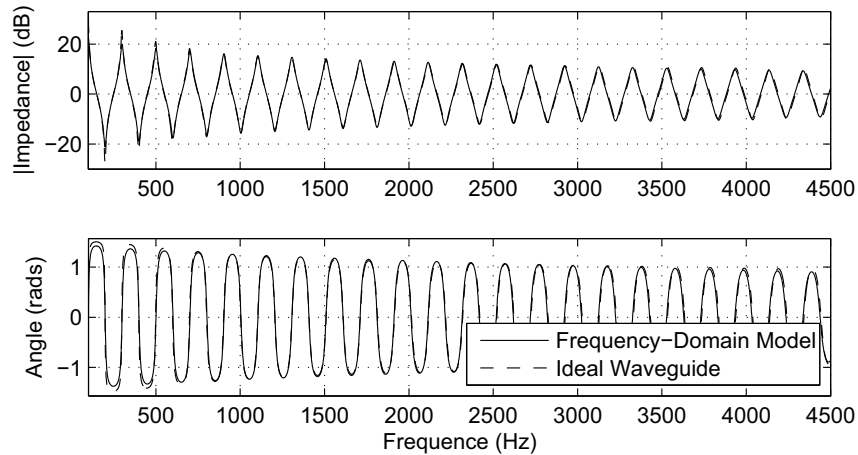


Figure 4.22 The input impedance of a long cylinder predicted using a frequency-domain model plotted against input impedance calculated from an ideal waveguide model.

The difference between the waveguide simulation and the frequency domain approach is similar to the short cylinder and simulations integrating the diameter discontinuity introduce the same offset in the impedances. With no discontinuity in the waveguide, windowing the reflection function also does not change the calculated impedance significantly.

With simulations of a reflecting source and diameter discontinuity, the windowed reflection function again yields a significantly different input impedance. The input impedance calculated from this model, with the same -5.53 dB offset as before, plotted against the theoretically predicted impedance is shown in Fig. 4.23.

Even with the longer tube, the impedance calculated using the first 696 samples of the reflection function is very close to the theoretically predicted impedance. Because the results are so similar, the difference between this impedance and the theoretically predicted one is shown in Fig. 4.24.

The differences has a similar shape as the difference found with the short cylinder model shown in Fig. 4.17. Again the largest differences are at resonances and anti-resonances below 2000 Hz, however the anti-resonances in that region are lower than predicted by the frequency domain approach and the resonances are higher than predicted, exactly the opposite of the short cylinder results from in Section 4.2.1.

Differences at the first few resonances and anti-resonances are no larger than with the smaller cylinder model, however the diversion from theoretical values between resonances and anti-resonances is greater. The impedance was calculated again from the waveguide model, this time doubling the length of both the calibration and measurement windows, simulating the inclusion of a reflection from the source, like at the end of Section 4.2.1. The impedance calculated this way is plotted against the ideal waveguide impedance in

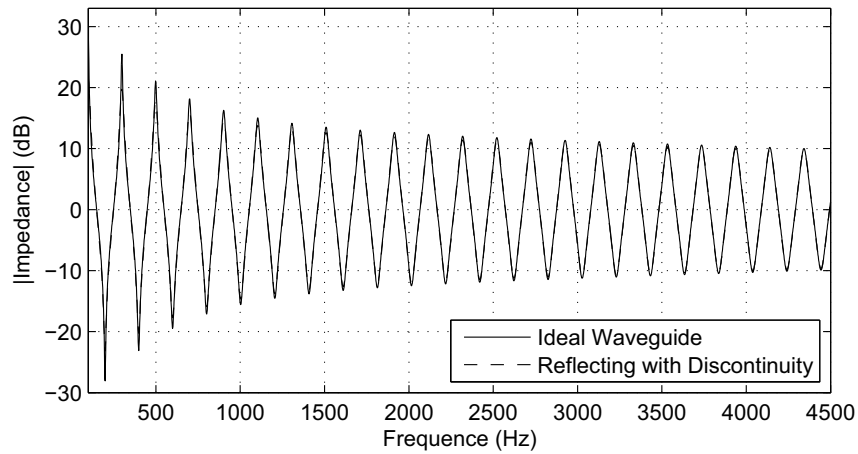


Figure 4.23 The input impedance of the longer cylinder calculated from an ideal waveguide simulation and input impedance calculated from a waveguide modelling a reflecting source and a diameter discontinuity.

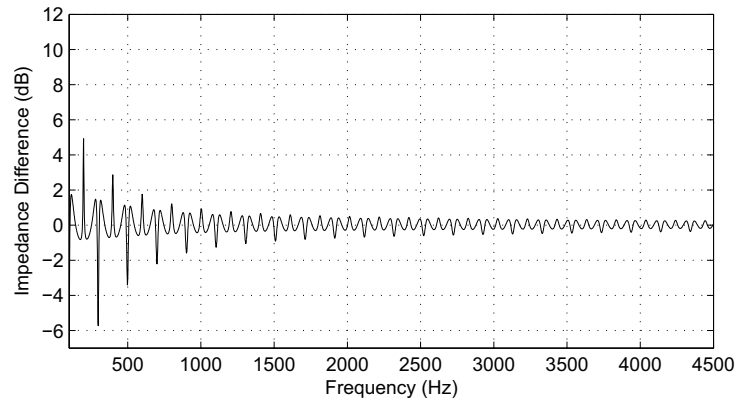


Figure 4.24 The magnitude difference between the input impedance calculated from an ideal waveguide simulation and input impedance calculated from a waveguide incorporating a reflecting source and scattering junction.

Fig. 4.25 and the difference between the two is shown in Fig. 4.26.

Including the source reflections in the model causes a lot of distortion in the low frequency impedances, shifting and smearing the resonances and anti-resonances. Even above about 1000 Hz, where the results are generally closer to the predicted values, the difference is less uniform and smoothly varying than in Fig. 4.24.

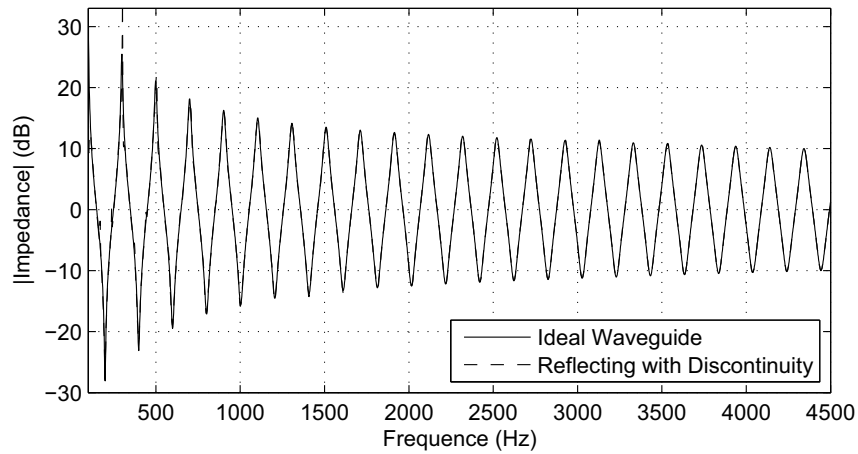


Figure 4.25 The input impedance of the longer cylinder calculated from an ideal waveguide simulation and the input impedance calculated by incorporating source reflections from a waveguide modelling a reflecting source and a diameter discontinuity.

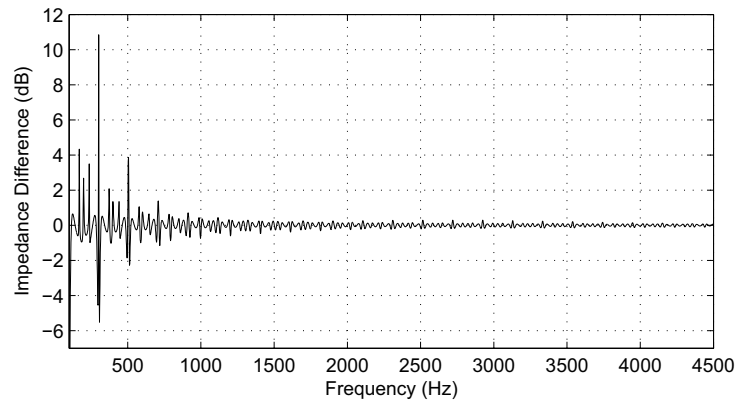


Figure 4.26 The magnitude difference between the input impedance calculated from an ideal waveguide simulation and input impedance calculated by incorporating source reflections from a waveguide modelling a reflecting source and diameter discontinuity.

Measured Results

Measurements for the longer cylinder were conducted in the same session as those for the short cylinder in Section 4.2.1. The reflection function was first measured until reflections from the source returned to the microphone. The input impedance calculated from this reflection function, with the same -3.7 dB offset as before, is plotted against the impedance

predicted by a frequency-domain model in Fig. 4.27.

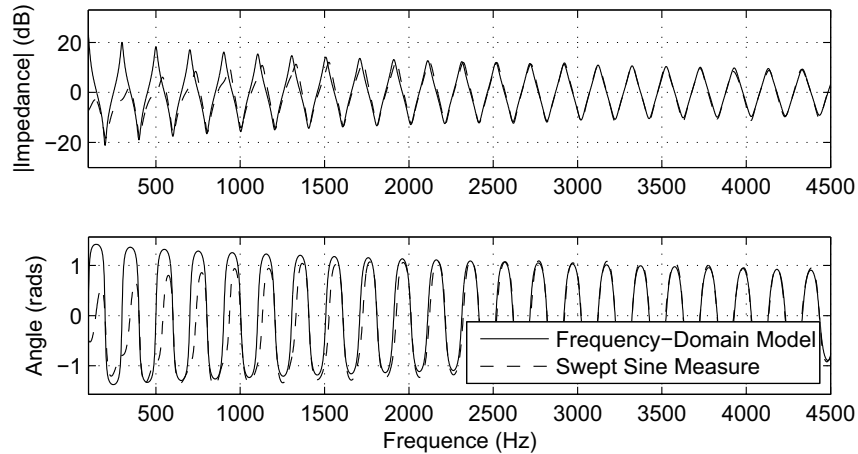


Figure 4.27 The input impedance of the long cylinder predicted from a frequency-domain model and calculated from measurements taken from a pulse reflectometry apparatus.

Resonances below 2000 Hz are visibly diminished compared to the predicted values and the anti-resonances are also significantly less extreme than predicted. The positions of the resonances below 2000 Hz are also inconsistent with the resonances of those above. The difference between the impedance calculated from the measurements and the one predicted by theory is plotted in Fig. 4.28.

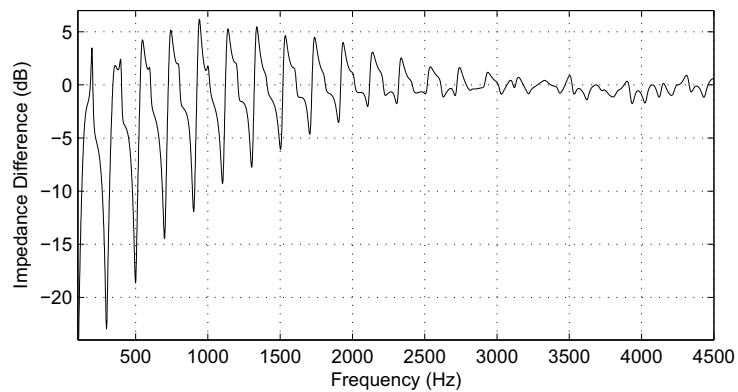


Figure 4.28 The magnitude difference between the input impedance predicted from a frequency-domain model of the long cylinder and the input impedance calculated from measurements taken from a pulse reflectometry apparatus.

Because of the shifted location of the peaks, this plot differs dramatically from the prediction in Fig. 4.24. The maximal and minimal differences are still at the resonances and anti-resonances, but because of the distorted locations of the peaks the shape is quite different. The resonances are lower than predicted and the anti-resonances are higher, as was the case in the model.

Source Reflections

Increasing the analysis window to include the first reflections off the source produced impedances which again are nominally closer to the theoretically predicted values.

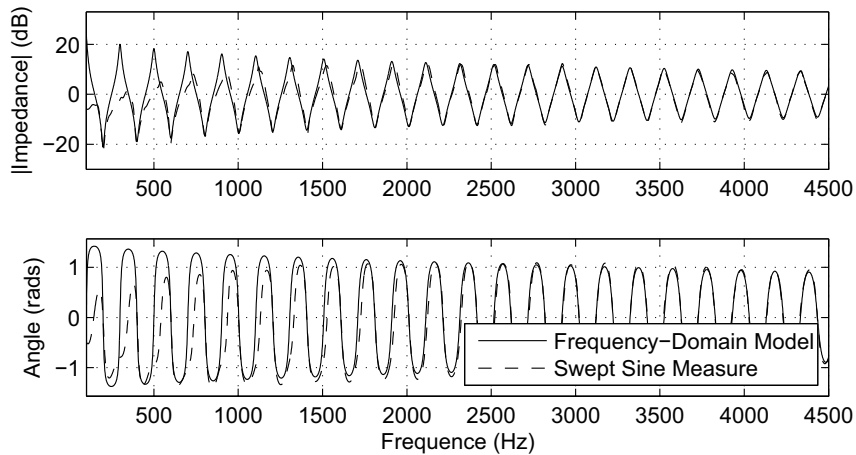


Figure 4.29 The input impedance of the long cylinder predicted from a frequency-domain model and calculated from measurements taken from a pulse reflectometry apparatus.

We see again that simply doubling the window size does not drastically reduce the difference between the impedance from the measurements and the theoretically predicted impedance and that in some respects the newly calculated impedance is less accurate. The difference between this impedance and the theoretical predicted impedance is shown in Fig. 4.30.

The lack of improvement between the two shown here implies that the reflection function of the long cylinder in the presence of a diameter discontinuity is still too long for the measurement window of $T_{S-M} + T_{M-O}$ and that significant truncation is still occurring.

It is possible to predict when this truncation will occur ahead of time by calculating the theoretical length of the impulse response of the object to be measured ahead of time and comparing this to T_{S-M} , however one should be careful to include the way the scattering junction increases the reflection function length.

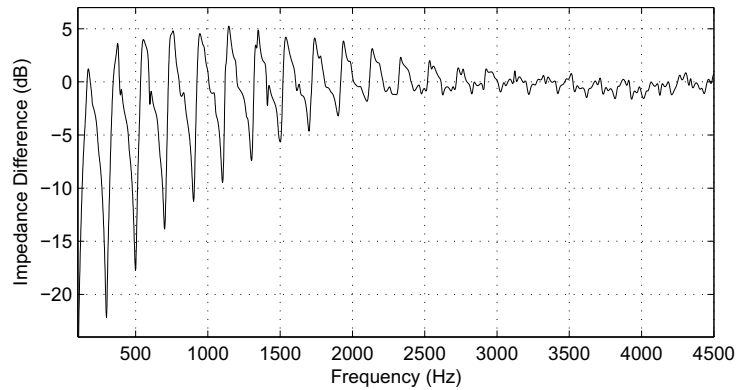


Figure 4.30 The magnitude difference between long cylinder input impedances calculate using frequency domain model and measured from pulse reflectometry with a double-sized window.

4.3 Conclusions

It is possible to use long signals as stimuli for a pulse reflectometry system, greatly increasing the measurement's resistance to polluting factors such as environmental noise and non-linearities. Impedances of real cylinders calculated from measurements taken with these signals closely match the theoretically predicted values over a large range of frequencies.

It is also possible to slightly increase the accuracy of impedances calculated from objects whose reflection functions are too long by incorporating reflections from the source into impedance calculations, however it is much more accurate to reduce the reflection function length by carefully matching the diameter of the source tube and object.

Chapter 5

Impedance Measurement Results

5.1 Measurements

In this chapter all measurements were performed in one session at 22.4 degrees Celsius to minimize environmental variances. A single linearly swept sine was created for the measurements and then played twice through the apparatus. The response to the second stimulus was taken with the stimulating signal then deconvolved from the measurement.

5.1.1 Viscothermal Losses

A calibration measurement was taken with the pulse reflectometry system to test that the rigid termination sufficiently acted as an infinite impedance reflector. For this comparison the pulse shape $f(t)$ was windowed out of the microphone signal and was deconvolved from the measurement of $r_o(t)f(t)$. The result of this deconvolution is shown in Fig. 5.1.

As expected the plot shows attenuation of energy increasing exponentially with frequency and is generally smooth until above 13 kHz, where higher modes of the duct are active. There is also a significant notch at around 9500 Hz which is present in the all of the pulse reflectometry microphone signals before deconvolution of the stimulus signal. If the microphone is detached from the measurement apparatus to take a measurement of the room the 9500 Hz signal is not present, implying that it is coming from either the driver, tube or headphone output of the DAC.

5.1.2 Open End Measurements

Next the rigid termination was removed and the source tube was left open to attempt to measure the reflectance of the open-end of an unflanged pipe. The open-end reflection function is very short and thus will be unaffected by windowing.

The calibration pulse measured in the last section was deconvolved from the pulse returning from the open end of the tube, and is plotted as a magnitude of reflectance

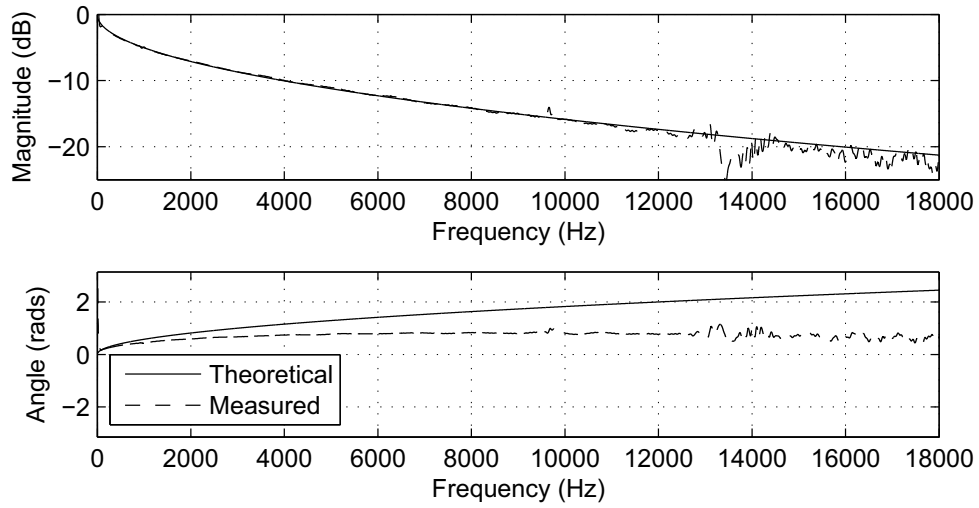


Figure 5.1 Measured magnitude and phase losses over T_{M-O} .

and as an end correction value of l/a against the value theoretically predicted by Levine and Schwinger (1948) in Fig. 5.2.

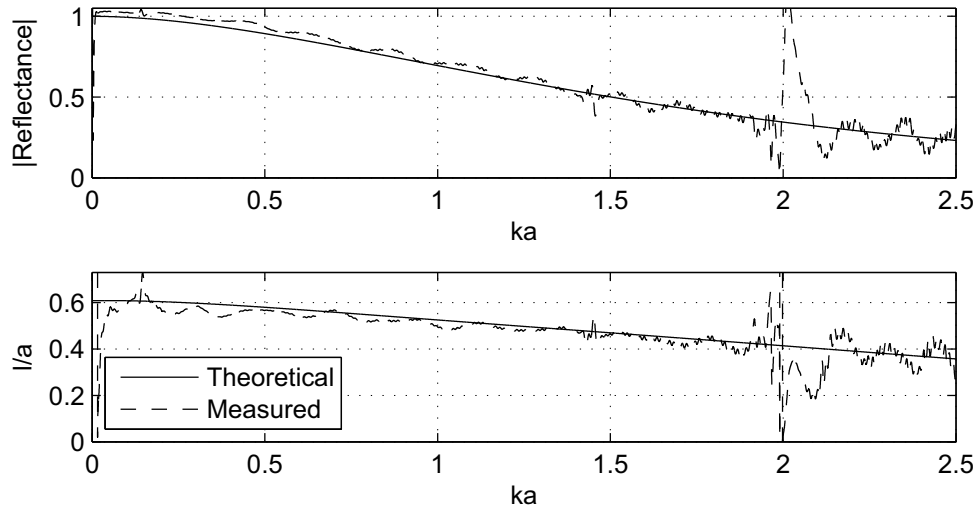


Figure 5.2 The reflectance magnitude and end length correction measured from the open end of the source tube.

The values are plotted against ka , where k is the propagation constant of sound in free

space defined by

$$k = \frac{2\pi}{\lambda} = \frac{2\pi f}{c}, \quad (5.1)$$

and a is the radius of the pipe. We can see that the measured reflectance and end length correction are fairly good matches with the predicted value at lower frequencies. As discussed in Chapter 2, measurements are only valid below the cut-on frequency of higher-order modes for the duct, which can be expressed as a ka value by solving Eq. 5.1 for f and substituting it into Eq. 2.6, yielding:

$$\begin{aligned} \frac{kc}{2\pi} &= \frac{1.84c}{2\pi a} \\ k &= \frac{1.84}{a} \end{aligned}$$

The large variation between the measured and the theoretically predicted reflectances start at around $ka = 1.9$ in Fig. 5.2, supporting this prediction.

5.1.3 Mouthpiece Measurements

A custom adaptor was built to allow the attachment of an alto saxophone mouthpiece to the end of the measurement probe. The adaptor consisted of a short extension pipe with a piece of cork around the outside over which the mouthpiece was inserted. Instead of rigidly terminating the end of the original source tube, the calibration is then done with a termination at the end of the adaptor, "calibrating out" the junction between the source tube and mouthpiece adaptor.

Closed Mouthpiece Measurements

Input impedance measurements were taken of five different saxophone mouthpieces: Caravan, Meyer 5, Meyer 8, Rascher and Selmer.

The saxophone mouthpieces were attached to the mouthpiece adaptor in turn and held firmly closed by pressing down on the reed using a thumb. For each of the measurements the same reed and ligature were used and moved progressively onto each mouthpiece. Each mouthpiece was inserted so that the end of the mouthpiece reached the same position on the adaptor.

Other Mouthpiece Measurements

The Selmer mouthpiece was then taken and measured in three other possible configurations. First the mouthpiece was measured in a completely open, undamped situation without thumb pressure on the reed.

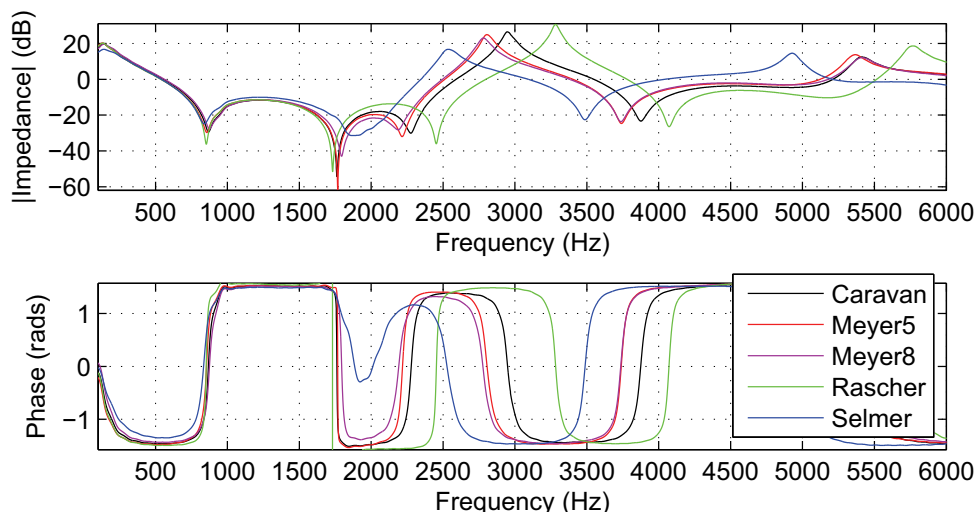


Figure 5.3 Input impedances measured from Caravan, Meyer, Rascher and Selmer mouthpieces while the reed was held closed.

Tape was then attached very lightly around the sides of the mouthpiece so that the reed was moved as little as possible from the undamped position while ensuring that the reed remained stationary during measurements. Additionally, when the measurements were taking place, thumb pressure was applied very lightly on the top of the reed to try and dampen any oscillations that might be induced.

Next, the tape was pulled tighter, so that the reed was open about half as much as it had been in the previous measurement. No thumb pressure was applied in this measurement situation, as the tape provided ample pressure on the reed to dampen it.

The impedance plot in Fig. 5.4 shows that the measurement with the reed open and undamped has sharp peaks at around 1300 Hz and 3600 Hz which are not present in the other measurements. Figure 5.5 shows the tail of the response of each of the mouthpieces after the stimulus signal is deconvolved from the primary measurement. These correspond to the resonances of the open and undamped reed.

Deconvolution of the calibration measurement was not done for the time-domain plot, because the time-domain result contained a lot of extraneous noise, however we can make comparative measures between the different mouthpiece configurations without deconvolving the apparatus characteristics, which should be present in all measurements.

When the reed is left open and undamped there is a significant tail to the response which is not present in any of the damped configurations. The period of this tail is between 0.74 ms and 0.83 ms, or a frequency range of 1205 Hz to 1351 Hz, corresponding to the peak present on the impedance plot.

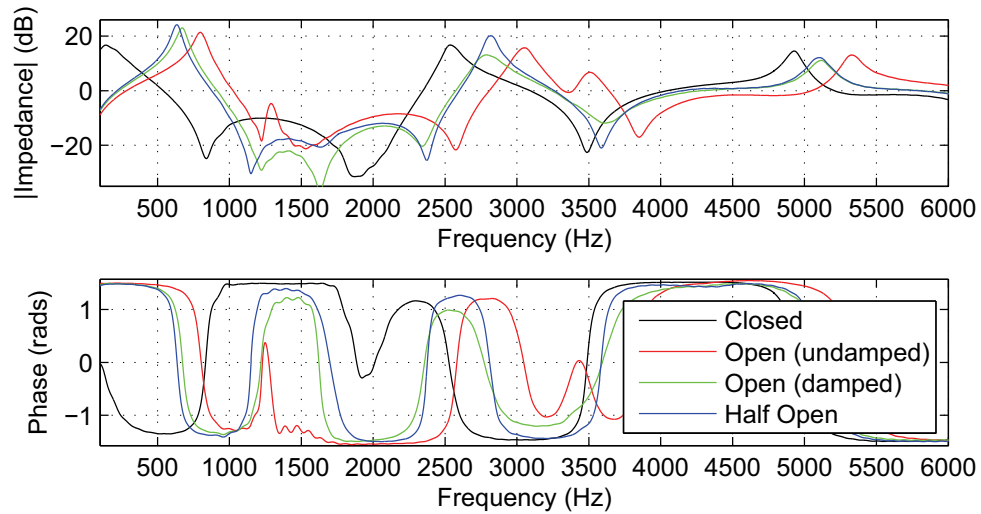


Figure 5.4 Input impedances from the Selmer mouthpiece while in various states.

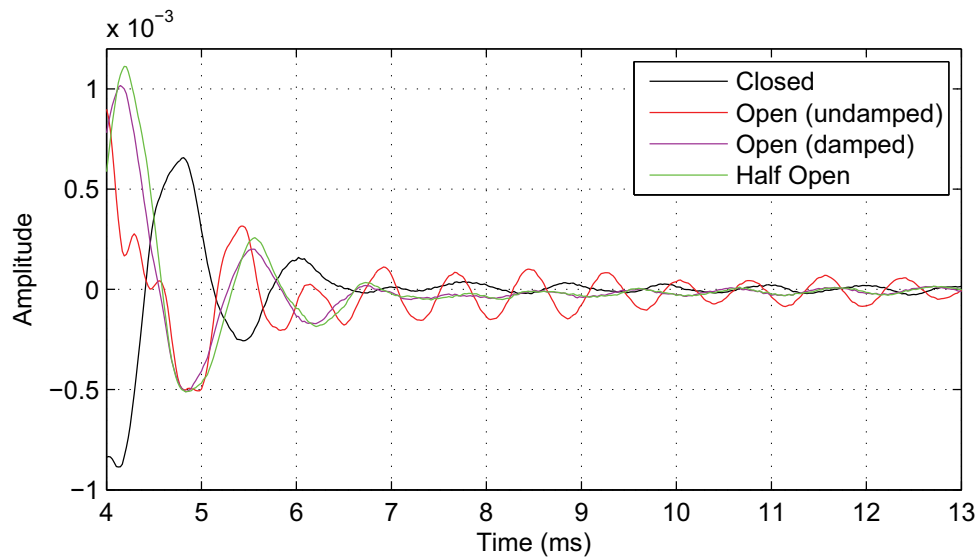


Figure 5.5 Zoom in on the tail of the pressure response of the Selmer mouthpiece in various states.

5.1.4 Mouthpiece Measurement Issues

The mouthpiece measurements presented in this section were completed by inserting each of the mouthpieces so that the base lined up to a common spot on the mouthpiece adaptor.

While that means the experiments are more easily repeatable, it means the locations of many of the resonant peaks may be shifted from their positions under normal use.

Because the mouthpiece will be adjusted by the player to correct the tone of the instrument, not all mouthpieces will be inserted to the same distance. This means the actual values for resonances, which can shift dramatically with small adjustments of the mouthpiece, may be significantly different from the measurements here.

Chapter 6

Conclusions

The work presented shows that it is possible to use extremely long stimulus signals in a pulse reflectometry setup to measure reflection functions. If the signal is carefully fed to the system and deconvolved from the response, stimuli much longer than the length of the source tube can be used to probe the objects under test, increasing the signal to noise ratio of the measurements dramatically.

Tests using a waveguide model presented in Section 4.1.2 also predict that a slowly swept sine wave yields the most accurate results in most measurement scenarios. The immunity to non-linearities, flexibility in creation and high signal-to-noise ratio that can be achieved compared to other methods all make it preferable to the other signal types presented. These tests also give us a rudimentary way to predict how non-ideal measurement situations will change measured reflectances.

The measurements at the end of Chapter 4 confirm many of the limitations when calculating impedance from objects whose reflection functions are too long for a given pulse reflectometry setup. As expected, the variations between the theoretical and measured results are greatest at the resonances and anti-resonances at low frequencies. The effects of the diameter discontinuities between the source tube and object were also measured and found to be significant. Even if the source tube is terminated anechoically the calculated impedance is offset and with a reflecting source the variations become unpredictable, especially with longer objects. Because it greatly reduces the reflection function length, matching the diameter between the source tube and object under study looks like the easiest way to measure longer objects more accurately.

Chapter 5 confirms that the pulse reflectometry system can reasonably measure viscothermal losses over the source tube and also does an adequate job of measuring the reflectance of the open end of an unflanged pipe. These measures are similar to their predicted values, greatly legitimizing the pulse reflectometry system as an accurate measurement system.

Input impedances of several saxophone mouthpieces are also presented showing similar impedances for many of the similarly sized mouthpieces. The largest variations between

the calculated impedances occur between mouthpieces which are vastly different in size.

Multiple impedance plots for the Selmer mouthpiece were presented. These plots show the mouthpiece response when the vibration of the reed is damped in three different states (closed, open and half-open) and once when the reed is left free. When the reed is undamped a reed resonance appears in the impedance plot which is clearly visible in a plot of the time-domain measurement before deconvolution of the calibration measurement.

6.1 Future Work

The conclusions of Section 4.1.2 are based on model data only and could be further verified by actual measurements, especially how non-linearity affects calculated impedances.

Bore reconstructions could be made in the presence of real DC offsets, comparing the ability of MLSs and sine sweeps to reconstruct a bore profile. Because the system uses standard audio hardware, a DC offset will likely not affect measurements however this could be experimentally verified.

Experiments using couplers which taper smoothly between the source tube and object diameter should be constructed to try to measure objects with longer reflection functions. Because it is not possible to increase the length indefinitely, some of the limitations with the current physical measurement apparatus could be avoided by limiting the discontinuity, which greatly increases the reflection function length.

The mouthpiece measurements of Chapter 5 were done in such a way that they could be easily repeated by a non-musician by inserting each one to the same spot in the measurement device. This is an unrealistic condition for a played instrument and measurements of the mouthpieces should be performed with a skilled player adjusting each mouthpiece on a saxophone by ear and then measuring the insertion distance.

With these distances to insert each mouthpiece as a guide more realistic comparisons can be made between input impedances measured from them, since some of the locations of the peaks would change dramatically when the insertion amount was set using the ear of a skilled player.

If couplers are constructed so that the measured objects sit flush with the source tube, then it will be possible to measure longer or more complex objects, such as cones. Also measurements of actual instrument cavities, including woodwind necks and bodies could be measured and compared against theoretically predicted values. Measurements between different manufactured versions of the same pieces, for example a comparison of saxophone necks from different makers, could also be investigated.

The time-domain response and calculated input impedances could also be given for different fingerings of instruments to compare how each playing state affects the input impedance of the body.

References

- ABEL, J. AND BERNERS, D. Lecture notes 5 - impulse response measurement. Lecture Notes for MUS424: Signal Processing Technique for Digital Audio Effects at Stanford University, 2004.
- ABEL, J. S. AND SMITH, J. O. Robust design of very high-order allpass dispersion filters. In *Proc. of the 9th Int. Conference on Digital Audio Effects (DAFx-06)* (Montreal, Canada, 2006).
- AOSHIMA, N. Computer-generated pulse signal applied for sound measurement. *J. Acoust. Soc. Am.* 69 (1981), pp. 1484–1488.
- BENADE, A. AND IBIS, M. Survey of impedance methods and a new piezo-disk-driven impedance head for air columns. *J. Acoust. Soc. Am.* 81, 4 (1987), pp. 1152–1167.
- BENADE, A. H. The physics of brasses. *Scientific American* 229, 1 (1973), pp. 24–35.
- BENADE, A. H. AND SMITH, J. H. Brass wind instrument impulse response measurements. *J. Acoust. Soc. Am.* 70, S1 (1981), pp. S22–23.
- BUICK, J., KEMP, J., SHARP, D., VAN WALSTIN, M., CAMPBELL, D. AND SMITH, R. Distinguishing between similar tubular objects using pulse reflectometry: a study of trumpet and cornet leadpipes. *Meas. Sci. Technol.* 13 (2002), pp. 750–75.
- DALMONT, J.-P. Acoustic impedance measurement, part I: A review. *Journal of Sound and Vibration* 243, 3 (2001), pp. 427–439.
- DAVIES, W. Generation and properties of maximum-length sequences, parts (1-3). *Control* 10 (1966), pp. 302–304, 364–365, 431–433.
- ELLIOT, S., BOWSER, J. AND WATKINSON, P. Input and transfer response of brass wind instruments. *J. Acoust. Soc. Am.* 72, 6 (1982), pp. 1747–1760.
- FARINA, A. Simultaneous measurement of impulse response and distortion with a swept-sine technique. In *Proceedings of the 108th AES Convention* (Paris, 2000).

- FOSTER, S. Impulse response measurement using Golay codes. In *Proceedings of IEEE International Conference on Acoustics, Speech, and Signal Processing '86* (1986).
- FREDBERG, J., WOHL, M., GLASS, G. AND DORKIN, H. Airway area by acoustic reflections measured at the mouth. *J. Appl. Physiol.* 48, 5 (1980), pp. 749–758.
- GRIESINGER, D. Impulse response measurements using all-pass deconvolution. In *Proceedings of the 11th International AES Conference* (Portland, Oregon, 1992).
- JACKSON, A., BUTLER, J., MILLET, E., HOPPIN, F. AND DAWSON, S. Airway geometry by analysis of acoustic pulse response measurements. *J. Appl. Physiol.* 43, 3 (1977), pp. 523–536.
- KEEFE, D. H. Acoustical wave propagation in cylindrical ducts: Transmission line parameter approximations for isothermal and nonisothermal boundary conditions. *J. Acoust. Soc. Am.* 75, 1 (1984), pp. 58–62.
- KEEFE, D. H. Wind-instrument reflection function measurements in the time domain. *J. Acoust. Soc. Am.* 99, 4 (1996), pp. 2370–2381.
- KELLY, JR., J. L. AND LOCHBAUM, C. C. Speech synthesis. In *Proc. Fourth Int. Congress on Acoustics* (Copenhagen, Denmark, 1962). Paper G42.
- LEVINE, H. AND SCHWINGER, J. On the radiation of sound from an unflanged circular pipe. *Physical Review* 73, 4 (1948), pp. 383–406.
- MARSHALL, I. Acoustic reflectometry with an arbitrarily short source tube. *J. Acoust. Soc. Am.* 91, 6 (1992), pp. 3558–3564.
- MÜLLER, S. AND MASSARANI, P. Transfer-function measurement with sweeps. *J. Audio Eng. Soc.* 49, 6 (2001), pp. 443–471.
- PAGNEUX, V., AMIR, N. AND KERGOMARD, J. A study of wave propagation in varying cross-section waveguides by modal decomposition. part I. theory and validation. *J. Acoust. Soc. Am.* 100, 4 (1996), pp. 2034–2048.
- PRATT, R., ELLIOTT, S. AND BOWSER, J. The measurement of the acoustic impedance of brass instruments. *Acustica* 38 (1977), pp. 236–246.
- RIFE, D. D. Transfer-function measurement with Maximum-Length Sequences. *J. Audio Eng. Soc.* 37, 6 (1989), pp. 419–444.
- SCAVONE, G. P. *An Acoustic Analysis of Single-Reed Woodwind Instruments with an Emphasis on Design and Performance Issues and Digital Waveguide Modeling Techniques*. PhD thesis, Stanford University, 1997.

- SHARP, D. B. *Acoustic pulse reflectometry for the measurement of musical wind instruments*. PhD thesis, University of Edinburgh Institute of Technology, 1996.
- SONDHI, M. M. AND GOPINATH, B. Determination of vocal-tract shape from impulse response at the lips. *J. Acoust. Soc. Am.* 49, 6 (1971), pp. 1867–1873.
- SONDHI, M. M. AND RESNICK, J. The inverse problem for the vocal tract: Numerical methods, acoustical experiments, and speech synthesis. *J. Acoust. Soc. Am.* 73, 3 (1983), pp. 985–1002.
- STAN, G.-B., EMBRECHTS, J.-J. AND ARCHAMBEAU, D. Comparison of different impulse response measurement techniques. *Journal of the Audio Engineering Society* 50, 4 (2002), pp. 249–262.
- SUZUKI, Y., ASANO, F., KIM, H.-Y. AND SONE, T. An optimum computer-generated pulse signal suitable for the measurement of very long impulse responses. *J. Acoust. Soc. Am.* 97, 2 (1995), pp. 1119–1123.
- SVENSSON, U. P. AND NIELSEN, J. L. Errors in MLS measurements caused by time variance in acoustic systems. *J. Audio Eng. Soc.* 47, 11 (1999), pp. 907–927.
- VAN WALSTIJN, M., CAMPBELL, M., KEMP, J. AND SHARP, D. Wideband measurement of the acoustic impedance of tubular objects. *Acta Acustica United with Acustica* 91 (2005), pp. 1–15.
- VANDERKOOY, J. Aspects of MLS measuring systems. *J. Audio Eng. Soc.* 42, 4 (1994), pp. 219–231.
- WARE, J. A. AND AKI, K. Continuous and discrete inverse-scattering problems in a stratified elastic medium. *J. Acoust. Soc. Am.* 45, 4 (1969), pp. 911–921.
- WATSON, A. AND BOWSER, J. Impulse measurements on brass musical instruments. *Acustica* 66 (1988), pp. 170–174.
- ZHOU, B., GREEN, D. M. AND MIDDLEBROOKS, J. C. Characterization of external ear impulse responses using Golay codes. *J. Acoust. Soc. Am.* 92, 2 (1992), pp. 1169–1171.